Control of Superconductivity in a Hybrid Superconducting/Ferromagnetic Multilayer Using Nonequilibrium Tunneling Injection*

S. Shafranjuk,[1] I. P. Nevirkovets,[2] O. A. Mukhanov,[2] and J. B. Ketterson[1,3]

[1]*Department of Physics and Astronomy, Northwestern University, Evanston, Illinois 60208, USA*
[2]*Hypres, Inc., Elmsford, New York 10523, USA*
[3]*Department of Electrical Engineering & Computer Science, Northwestern University, Evanston, Illinois 60208, USA*

(Received 5 November 2015; revised manuscript received 21 March 2016; published 26 August 2016)

We report a theoretical and experimental study on the use of nonequilibrium tunneling injection to control the local Cooper pair amplitude Φ_S in an SF sandwich involving superconducting (S) and ferromagnetic (F) layers coupled by the proximity effect. In an $SISFIFS$ structure (where I is an insulator), this same SF sandwich serves as the acceptor electrode of an $SISF$ Josephson junction whose critical current I_{ca} depends on Φ_S. We derive the self-consistency equation describing the critical temperature T_c of the SF sandwich under nonequilibrium conditions. In addition, we compute I_{ca} by solving the Boltzmann equation for the electron distribution function f_ε, which then allows a determination of the relative change of $\delta I_{ca}/\delta I_i(V_i)$ versus the bias voltage V_i and the injection current $I_i(V_i)$. The computed gain $\delta I_{ca}/\delta I_i(V_i)$ strongly depends on $\delta I_{ca}/\delta I_i(V_i)$, and agrees well with the experimental data.

DOI: 10.1103/PhysRevApplied.6.024018

I. INTRODUCTION

Progress towards next-generation computing is rapidly approaching a crisis due to thermal management and other issues associated with semiconductor technologies [1]. New device and computing strategies with significantly higher energy efficiencies are clearly required [2,3]. Cryogenic superconducting single-flux quantum (SFQ) technologies with switching energies $\sim 10^{-19}$ J/bit are actively being pursued as a basis for future processors [4,5]. However, dense and energy-efficient memories compatible with SFQ logic have yet to be developed. Promising cryogenic memory technologies based on magnetic memory devices have been considered [6–10]. The challenge of combining superconducting processing devices and magnetic memory arrays in a single circuit requires matching substantially different material and electrical characteristics. A promising approach involves the direct integration of materials with competing-order parameters in *multilayered structures*. Superconductor/ferromagnet heterostructures allow one to exploit additional mechanisms to control the superconducting state, thereby considerably expanding the functionality of existing devices and possibly leading to the development of completely new ones [11,12].

The focus of the present work is to develop the theory of quasiparticle-injection devices [13–23] which are modified to include ferromagnetic layers. It is anticipated that such devices will find various applications in superconducting electronics [24–26], and improving their performance will require a better understanding of the physics of the nonequilibrium superconducting (S) state in hybrid multilayered structures.

Excess nonequilibrium excitations in an S layer, which tend to occupy all the available electron states, lead to a weakening of Cooper pairing, thereby causing the suppression of the superconducting correlations. This allows one to establish control of the superconducting state by injecting quasiparticle excitations from an adjacent electrode through a tunnel junction [13–23]. A particular device exploiting this approach was proposed by Faris [15] and is known as the quiteron. In this three-terminal device, the two Josephson junctions are stacked on top of each other to form an $S_1IS_2IS_3$ structure (where I is an insulating tunnel barrier). When biased above the sum-gap voltage, the S_2IS_3 junction injects excess quasiparticles into the S_2 electrode, thereby suppressing superconductivity in that layer. Since the S_2 electrode is shared by the acceptor (S_1IS_2) junction, the $I-V$ curve of the acceptor junction is perturbed. For the same reason, if a voltage is applied across the acceptor junction, the $I-V$ curve of the injector junction is affected. This backaction is undesired and has to be suppressed for the device to be used in superconducting circuits. One way to do this is to suppress the superconducting correlations in the injector junction in the vicinity of the barrier.

In previous publications the authors have shown that introducing very thin ferromagnetic (F) layers on both

*The views and conclusions contained herein are those of the authors and should not be interpreted as necessarily representing the official policies or endorsements, either expressed or implied, of the ODNI, IARPA, or the U.S. Government. The U.S. Government is authorized to reproduce and distribute reprints for Governmental purposes notwithstanding any copyright annotation thereon.

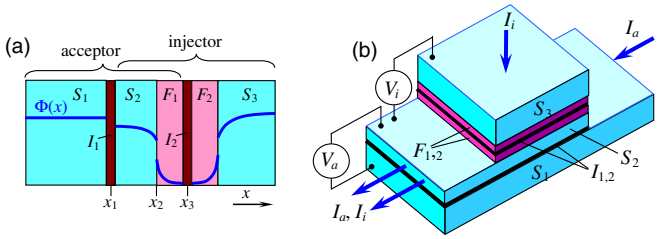

FIG. 1. (a) The hybrid multilayer device wherein superconductivity in S_2 layer and the Josephson current through the $S_1I_1S_2F_1$ junction (acceptor) are controlled by injecting nonequilibrium quasiparticles via the $S_2F_1I_2F_2S_3$ junction (injector). The Cooper pair amplitude $\Phi(x)$ (where x is the coordinate perpendicular to the layers) is shown by the blue line; it is discontinuous at the S_2F_1 and F_2S_3 interfaces and vanishes near the tunneling barrier I_2, leading to a suppression of the Josephson supercurrent component inside the injector. (b) Schematic view of the device (not to scale) and biasing used in the experiment.

sides of the injector barrier efficiently eliminates both the Josephson current flowing through the injector junction and the gap-related features in its $I-V$ curve [24–26], owing to the presence of the exchange field in F [27]. It is also shown that input-output isolation in the modified devices, designated superconducting-ferromagnetic transistors (SFTs), is greatly improved as compared with the quiteron [24–26].

In order to provide a theoretical basis for optimizing the characteristics of the devices studied here, we consider how to control the Josephson current flowing through the $S_1I_1S_2F_1$ (the left or acceptor) junction of the multilayered hybrid structure shown in Fig. 1. The structure involves three superconducting (S), two insulating (I), and two ferromagnetic (F) layers. The blue line in Fig. 1 denotes the spatial dependence of the Cooper pair amplitude $\Phi(x)$. In the S_2F_1 sandwich, $\Phi(x)$ in S_2 is diminished due to the inverse proximity effect with adjacent F_1 layer. Additional suppression of $\Phi(x)$ in S_2 can be realized by injecting nonequilibrium quasiparticles from the F_2S_3 electrode through the potential barrier I_2. Thus, excess quasiparticles injected from the F_2S_3 electrode into the middle S_2F_1 sandwich create conditions for a transition of the S_2 layer from the superconducting to normal state, which can be used to control the Josephson current through the acceptor junction.

II. EXPERIMENT

The multilayer SFT-device structure [see Fig. 1(b)] is implemented [24–26] in the vertically integrated form. This geometry allows one to efficiently utilize valuable chip space. The top superconducting S_3 electrode enables four-terminal-like measurements of the injector junction and minimizes the resistive contribution of the F layers. (The role of the F layers is discussed in more detail in our former publications [24–26].) Briefly, the role of these layers is to block superconducting correlations across the I_2 barrier. Simultaneously, the F_1 layer has to be thin enough to prevent significant quasiparticle trapping in it. A ferromagnetic material is chosen for F_1 because it is challenging to find a nonmagnetic N layer, which can satisfy the above two conditions simultaneously (an N layer could be used in place of F_2, but it is convenient to use the same material for both the F_1 and F_2 layers).

The devices are fabricated from $Nb_{(1)}/Al/AlO_x/Nb_{(2)}/Ni_{(1)}/Al/AlO_x/Ni_{(2)}/Nb_{(3)}$ multilayers deposited *in situ* onto oxidized Si substrates. Typical thicknesses of the layers in the devices are as follows: 120, 42, and 80 nm for the $Nb_{(1)}$, $Nb_{(2)}$, and $Nb_{(3)}$ layers, respectively; 2.7 nm for $Ni_{(1)}$ layer; and 2.7–6.7 nm for the $Ni_{(2)}$ layer. Other important device parameters are listed below in Sec. IV. Our device geometry [see Fig. 1(b)] allows us to electrically bias the injector and the acceptor junction separately using two independent battery-powered current sources. The preamplifiers for the voltage signals are also battery powered in order to minimize external electromagnetic influences. The devices are characterized at 4.2 K in a shielded environment. We measure I_{ca} versus H dependences of the S_1IS_2 acceptor junction (where I_{ca} is the maximum dc Josephson current and H is an external magnetic field applied parallel to the layers) at different levels of the current I_i through the $S_2F_1I_2F_2S_3$ injector junction. The maximum I_{ca} is determined from the $I_{ca}(H)$ dependences and plotted against I_i.

III. MODEL FOR A MULTILAYERED HYBRID JUNCTION

Here, we propose a tractable theoretical model based on the nonequilibrium Green's function technique [28–30], which allows us to describe and interpret experimental data and with it provide theoretical guidance for the device optimization. We show that the superconducting correlations and Josephson current in hybrid multilayered structures (cf. Fig. 1) can be controlled by quasiparticle injection, so that reversible switching between the superconducting and resistive states can be realized. Because of the complexity of the system and various physical phenomena governing the device operation, a full self-consistent microscopic consideration of the problem requires a numeric approach. Unfortunately, the physical interpretation of the results obtained is not transparent, and for this reason, we simplify the theoretical model in order to obtain analytical solutions. Good agreement between the simplified theory and the experimental data confirms that our model captures the basic physics of the experimental device.

As noted, the nonequilibrium Green's functions [30] describing the superconducting properties and phase-coherent transport in the multilayered hybrid structure is rather complex. A tractable description becomes possible

by making simplifying assumptions based on the available experimental data. First, for the sake of convenience, we split the whole multilayered structure into several smaller pieces. The central part of the system is the S_2F_1 sandwich, which plays two important but different roles. On one hand, the S_2F_1 sandwich is the left electrode of the $S_2F_1I_2F_2S_3$ injector junction, where one creates a nonequilibrium distribution of quasiparticles. On the other hand, the same S_2F_1 sandwich is the right electrode of the $S_1I_1S_2F_1$ acceptor Josephson junction, whose critical current I_{ca} is controlled by changing the bias current I_i (or voltage V_i) across the injector. Second, our experimental data imply that the Josephson current vanishes for the injector junction at $x = x_3$ (where x is the coordinate perpendicular to the layers); hence, Φ vanishes on both sides of the tunnel barrier I_2 due to the exchange field h in the adjacent ferromagnetic layers F_1 and F_2. On the contrary, the pair amplitude $\Phi_2(x)$ in S_2 remains essentially unchanged when approaching the barrier I_1, but closer to the S_2F_1 interface (see Fig. 1), it becomes increasingly suppressed due to the proximity with F_1.

In this work we have disregarded any effects of the (possibly different) orientation of the magnetization of F layers, because the available experimental data (see, e.g., the I_c versus H dependences reported in Refs. [25,31]) indicate a very weak or no permanent magnetic moment orientation in our "soft" magnetic layers, unlike the pronounced magnetization switching effects reported, e.g., in Ref. [8] for the case of strongly magnetized F layers. For the same reason, we neglect the effect of the spin-polarized injection. Also, the F-layer configuration used in the experiment is unlikely to support the triplet superconducting correlations which require special conditions to be observed. On the other hand, our model adequately describes the experimental data without the need to include any exotic superconducting correlations, which justifies neglecting them in the model.

The experimental $I-V$ curve of the injector junction reflects two important facts which we use in building our model. First, since the current versus voltage is linear [25,31], we conclude that the injector current is due to the quasiparticle excitations only, while the Josephson component of the electric current is absent owing to the finite exchange field $h \neq 0$ of the F_1 and F_2 layers. Second, the injector conductance allows us to find the tunneling injection intensity α_V, which is given by Eq. (26) below and in Sec. 4 of the Appendix.

The basic equations of the model are derived using the Keldysh Green's function method [27–30], which is briefly reviewed in Sec. 1 of the Appendix. The model is simplified in the "dirty" limit [27,32,33] $l_i \ll \xi_i$, where the electron mean free path l_i in the ith layer is much shorter than the superconducting coherence length $\xi_i = \sqrt{v_{Fi} l_i/(6\pi T_{ci})}$, where i is the layer index, v_{Fi} is the Fermi velocity and T_{ci} is the superconducting critical temperature. In the dirty limit, the hybrid multilayered stack is described in terms of Usadel equations for the quasiclassical retarded (R) energy-integrated Green's functions G_i^R and F_i^R, complemented with a Boltzmann equation for the distribution function $f_\varepsilon^{(i)}$ of nonequilibrium electrons [30] in the ith layer (see also Sec. 4 in the Appendix). For the sake of simplicity, we assume that the pair amplitude Φ_1 in the S_1 layer is position independent, while the coordinate dependences of $\Phi_2(x)$ in the S_2 layer and $\Phi_1^F(x)$ in the ferromagnetic F_1 layer are discussed below. For the S_2F_1 sandwich, the Usadel equation for the pair amplitude $\Phi_i(x)$ versus coordinate x perpendicular to layers reads

$$\Phi_i = \frac{\pi T_{c2}}{\varepsilon G_i^R}[(G_i^R)^2\Phi_i']'\xi_i^2 + \Delta_i, \tag{1}$$

where i is the layer index and ε is the energy variable. The Cooper pair amplitudes Φ_i ($i = 1, 2$ is the layer index) are related with the retarded (R) quasiclassical Green's functions G_i^R and F_i^R as

$$G_i^R(\varepsilon) = \frac{\varepsilon}{\zeta_\varepsilon}, F_i^R(\varepsilon) = \frac{G_i^R\Phi_i}{\varepsilon} = \frac{\Phi_i}{\zeta_\varepsilon}, \tag{2}$$

which satisfy the Usadel equation (1), where F_i^R is the anomalous retarded function describing superconducting correlations in the ith layer, and $\zeta_\varepsilon = \sqrt{\varepsilon^2 - \Phi_i\Phi_i^*}$. The self-consistency equation is

$$\Delta_{1,2}\ln\frac{T}{T_{c1,2}} = \frac{1}{2}\int_{-\infty}^{\infty}\frac{\Phi_{1,2}G_{1,2}^R - \Delta_{1,2}}{\varepsilon}(1 - 2f_\varepsilon^{(1,2)})d\varepsilon, \tag{3}$$

where $\Delta_{1,2}$ are the energy gaps of the $S_{1,2}$ layers, $T_{c1,2}$ are their critical temperatures, and $f_\varepsilon^{(1,2)}$ are the nonequilibrium electron distribution functions, as determined from the corresponding Boltzmann equation as discussed in Sec. 4 of the Appendix. According to our experimental results, $\Delta_2 = 0.75\Delta_1$ [31], where $\Delta_{1,2}$ are the local values of superconducting energy gap in the $S_{1,2}$ layers on the left (1) and right (2) sides of the tunneling barrier I_1 located at $x = x_1$. Both $\Delta_{1,2}$ and $T_{c1,2}$ are strongly affected by the nonequilibrium injection, as well as by the proximity effect in the hybrid system, which influences the acceptor Josephson current, since the latter depends on the electron spectrum and critical parameters of the S_2 and F_1 layers. Although the energy gap and critical temperature of the $F_{1,2}$ layers are equal to zero due to the absence of Cooper coupling inside a ferromagnetic layer, the proximity-induced pair amplitude $\Phi_i(x)$ in the $F_{1,2}$ layers remains finite and dependent on the coordinate x. The Josephson current through the $S_1I_1S_2$ interface associated with the acceptor and positioned at $x = x_1$, is

$$I_{\rm ca} = \frac{\sigma_2}{2e}\frac{1}{\xi_2\gamma_B}\,{\rm Re}\int\limits_{-\infty}^{\infty}\frac{G_1^R G_2^R \Phi_1\Phi_2^*}{\varepsilon^2}(1-f_\varepsilon^{(1)}-f_\varepsilon^{(2)})d\varepsilon. \quad (4)$$

Here, σ_2 is the conductivity of S_2, $f_\varepsilon^{(1,2)}$ are the nonequilibrium electron distribution functions in $S_{1,2}$;

$$\gamma_B = \frac{2}{3}\frac{l_2}{\xi_2}\left\langle\frac{\Upsilon_B(\theta_B)\cos\theta_B}{1-\Upsilon_B(\theta_B)}\right\rangle_{\theta_2}^{-1} \approx \frac{2}{3}\frac{l_2}{\xi_2}\frac{1-\Upsilon_B}{\Upsilon_B} \quad (5)$$

is the parameter of the $S_1I_1S_2$ interface with transparency Υ_B [whose dependence on the electron incidence angle θ_B is sharp and here taken as $\Upsilon_B(\theta_B) = \Upsilon_B\delta(\theta_B)$]; $\langle\ldots\rangle_{\theta_2}$ implies averaging over θ_2 on the S_2 side in the vicinity of the S_2F_1 interface; $|x-x_2| < \xi_F$; $\xi_F = \sqrt{D_i^F/h}$ is the characteristic length of the superconducting correlation decay in the ferromagnetic layer F_i; and h and D_i^F are the exchange field and diffusion coefficient in F. According to the experiment, in the course of the tunneling injection we get $f_\varepsilon^{(1)} \simeq f_\varepsilon^{(2)} \neq f_\varepsilon^F$ where $f_\varepsilon^F = [\exp(\varepsilon/T)+1]^{-1}$ is the equilibrium Fermi-Dirac distribution at temperature T. At the S_2F_1 interface, the pair amplitudes $\Phi_2(x)$ in S_2 and Φ_1^F in F_1 satisfy the following boundary conditions [32,33]:

$$\begin{aligned} p_1^2 l_1^F G_1^2 \Phi_1^{F\prime} &= p_2^2 l_2 G_2^2 \Phi_2' \\ \xi_2\gamma_B G_2\Phi_2' &= G_1(\Phi_1^F - \Phi_2); \end{aligned} \quad (6)$$

here, $p_{1,2}$ are electron momenta in the S_2 and F_1 layers, l_1^F and l_2 is the electron mean free path in the F_1 and S_2 layers, and we have omitted index R in G for brevity.

Equations (1)–(6) allow for a simplified analytical description of superconducting correlations in the acceptor in terms of the pair-breaking rate γ_0, which adequately describes transport properties of the S_2F_1 interface [27] by taking into account the influence of the magnetic F_1 layer on the superconducting properties of the S_2 layer. On one hand, one can see that the Josephson supercurrent (4) depends on the nonequilibrium electron distribution $f_\varepsilon^{(1,2)}$ in the $S_{1,2}$ layers, controlled by the injector. On the other hand, the superconducting correlations in the S_2 layer are influenced by the proximity effect between S_2 and F_1 layers. According to our experiment, in the absence of quasiparticle injection there is a finite energy gap $\Delta_2 \neq 0$ (specifically, $\Delta_2 = 0.75\Delta_1$, where $\Delta_1 = 1.2$ meV) in the electron excitation spectrum of the S_2 layer. The gap in the S_2 layer is only slightly suppressed (by about 25% compared to the S_1 value) mainly due to interaction with the adjacent magnetic F_1 layer. In addition, our experiment suggests that the transparency Υ_B of the S_1IS_2 interface positioned at $x = x_1$ is quite low, whereas the other S_2F_1 interface (located at $x = x_2$) is relatively transparent. Therefore, for the sake of simplicity, we assume that Δ_1 is coordinate independent, whereas the coordinate dependence of $\Delta_2(x)$ in the region $x_1 < x < x_2$ is relatively weak (except the vicinity of the S_2F_1 interface) and is considered below. Furthermore, an almost perfect linearity of the injector $I-V$ curve indicates that despite the fact that the ferromagnetic layers $F_{1,2}$ are quite thin ($d_F \ll \xi_2$), the superconducting correlations in F vanish completely due to the presence of an exchange field $h \neq 0$. A natural explanation to these experimental facts is that the coordinate dependence of $\Delta_2(x)$ is smooth in S_2, while at the S_2F_1 interface $\Delta_2(x)$ is sharply reduced, and vanishes inside F_1, because the Cooper coupling does not exist in the F layers.

It is convenient to take into account the influence of the proximity effect in the S_2F_1 sandwich on the Josephson critical current of the S_1IS_2 junction by introducing the pair-breaking rate γ_0, as suggested in Ref. [27]. In other words, we treat the effect of the ferromagnetic layer as an effective boundary condition. This approximation allows for taking into account the mutual influence of the S_2 and F_1 layers originating from the nonlocality of the Cooper pairs in S_2 on one hand, and the presence of spin-polarized electrons in F_2 on the other hand, thereby enabling a simplification of the description of the Josephson effect in the acceptor, affected by the nonequilibrium and proximity effects. Furthermore, for the sake of simplicity, we disregard the effect of the nonequilibrium spin injection into the acceptor, i.e., we assume that in the acceptor region, the nonequilibrium electron excitations are not spin polarized. The latter assumption is justified by the fact that the experimental data considered here do not manifest effects which may be associated with the injection of spin-polarized excitations, as is mentioned above.

First, taking into account that $\Delta_2 \neq 0$, we approximate the anomalous function by

$$F_2^R(x) = G_2\frac{\Phi_2}{\varepsilon} = \frac{\Delta_2}{\zeta_\varepsilon^{(0)}}\left(1-\frac{\beta_\varepsilon}{2}(x-x_1)^2\right), \quad (7)$$

where we assume that the spatial variation parameter $\beta_\varepsilon \ll 1$, $\zeta_\varepsilon^{(0)} = \sqrt{\varepsilon^2-\Delta_2^2}$ is the "kinetic energy" and

$$\beta_\varepsilon = \gamma_0\frac{2\Delta_2}{(\zeta_\varepsilon^{(0)})^2}\frac{1}{d_S^2}, \quad (8)$$

where $d_{S2} = x_2 - x_1$ is the thickness of S_2 layer. The pair-breaking rate γ_0 is introduced via the equality

$$F_2^R(x = x_2) = \frac{\Delta_2}{\zeta_\varepsilon}, \quad (9)$$

where $\zeta_\varepsilon = \sqrt{\varepsilon^2-(\Delta_2+\gamma_0)^2}$.Using Eqs. (7) and (9), one obtains

$$\frac{\Delta_2}{\zeta_\varepsilon} = \frac{\Delta_2}{\zeta_\varepsilon^{(0)}}\left(1 - \frac{\beta_\varepsilon}{2} d_{S2}^2\right), \tag{10}$$

thereby establishing a connection between γ_0 and β_ε in the form

$$\gamma_0^{(+)} \simeq \beta_\varepsilon \frac{(\zeta_\varepsilon^{(0)})^2}{\Delta_2}\frac{d_{S2}^2}{2},$$
$$\gamma_0^{(-)} \simeq -\frac{2\Delta(\zeta_\varepsilon^{(0)})^2}{\varepsilon^2 - 2\Delta_2^2} - \gamma_0^{(+)}. \tag{11}$$

We emphasize that the definition of the pair-breaking rate γ_0 is different from that in Ref. [27], since we take into account the finite value of $\Delta_2 \neq 0$ in S_2.

The value of γ_0 is deduced from the boundary conditions at the S_2F_1 interface. Taking into account that

$$\Phi_2(x) = \Delta_2\left(1 - \frac{\beta_\varepsilon}{2}(x - x_1)^2\right),$$
$$\Phi_2'(x) = -\Delta_2\beta_\varepsilon(x - x_1),$$
$$\frac{\Phi_2'(x_2)}{\Phi_2(x_2)} = \frac{-\Delta_2\beta_\varepsilon d_{S2}}{\Delta_2(1 - \frac{\beta_\varepsilon}{2}d_{S2}^2)} = -\frac{\beta_\varepsilon d_{S2}}{1 - \frac{\beta_\varepsilon}{2}d_{S2}^2} \simeq -\beta_\varepsilon d_{S2}, \tag{12}$$

we conclude that γ_0 is directly related to the logarithmic derivative of $\Phi_2(x)$ at the interface $x = x_2$:

$$\frac{\Phi_2'(x_2)}{\Phi_2(x_2)} \simeq -\beta_\varepsilon d_{S2} = -\gamma_0 \frac{2\Delta}{d_{S2}(\zeta_\varepsilon^{(0)})^2}. \tag{13}$$

Using for the S_2F_1 interface the boundary conditions in the form of Eq. (6), we obtain

$$\Phi_2' = \frac{p_1^2 l_1^F G_1^2}{p_2^2 l_2 G_2^2}\Phi_1^{F\prime} = \frac{\sigma_1^F}{\sigma_2}\Phi_1^{F\prime}$$
$$\Phi_2 = \Phi_1^F - \xi_2\gamma_B^F\frac{p_1^2 l_1^F G_1}{p_2^2 l_2 G_2}\Phi_1^{F\prime} = \Phi_1^F - \xi_n\gamma_B^F\Phi_1^{F\prime}, \tag{14}$$

where

$$\gamma_B^F = \frac{2}{3}\frac{l_1^F}{\xi_1^F}\frac{1 - \Upsilon_B^F}{\Upsilon_B^F} \tag{15}$$

is the parameter of the S_2F_1 interface with transparency S_2F_1; l_1^F is the electron mean free path in F_1; σ_1^F and σ_2 are the electric conductivities of the ferromagnetic layer F_1 and the superconducting layer S_2, respectively; $\Phi_1^{F\prime} = \partial\Phi_1^F/\partial x$; and following Ref. [27], in analogy with the superconducting coherence length $\xi_i = \sqrt{D_i/(2\pi T_c)}$ (where $D_i = v_{Fi}l_i/3$ is the diffusion coefficient in the ith layer), we introduced the normal metal coherence length $\xi_n = \sqrt{D_i^F/(2\pi T_{ci})}$, where D_i^F is the diffusion coefficient in a ferromagnetic layer. Equations (13) and (14) also give

$$\gamma_0 = -\frac{d_{S2}(\zeta_\varepsilon^{(0)})^2}{2\Delta_2}\frac{\Phi_2'(x_2)}{\Phi_2(x_2)}$$
$$= -\frac{d_{S2}(\zeta_\varepsilon^{(0)})^2}{2\Delta_2}\frac{\sigma_1^F}{\sigma_2}\frac{\Phi_1^{F\prime}(x_2)}{\Phi_1^F(x_2) - \xi_n\gamma_B\Phi_1^{F\prime}(x_2)}. \tag{16}$$

The pair-breaking rate γ_0 is readily computed using the explicit form of $\Phi_1^F(x)$ and $\Phi_1^{F\prime}(x)$, found as solutions of the Usadel equation. Here, we use the established experimental fact that the superconducting correlations vanish completely across the $F_1I_2F_2$ interface, which automatically means that Φ_1^F is small inside the F_1 and F_2 layers. Then, the linearized Usadel equation represents a good approximation for this case. Therefore, for the sake of convenience, we use the linearized Usadel equation [27] on $\Phi_1^F(x)$, considering that, in the F layers, $\Phi_1^F(x)$ is energy independent, and $F_{1,2}^R = \Phi_{1,2}^F/\varepsilon$. In the vicinity of the S_2F_1 interface (i.e., for $|x - x_2| < \xi_F$), the linearized Usadel equation at $x > x_2$ takes the form

$$ih\,\mathrm{sng}(\varepsilon)\Phi_1^F - \frac{D_1^F}{2}\Phi_1^{F\prime\prime} = 0. \tag{17}$$

At $\varepsilon > 0$, the decaying solution of Eq. (17) takes the form [27]

$$\Phi_1^F(x) = A\sinh\left(-\frac{i+1}{\xi_F}(x - x_2)\right) + B,$$
$$\Phi_1^{F\prime}(x) = -\frac{i+1}{\xi_F}A\cosh\left(-\frac{i+1}{\xi_F}(x - x_2)\right), \tag{18}$$

where coefficients A and B are obtained from the boundary conditions (6). For the highly transparent S_2F_1 interface, taking into account Eq. (8), and provided that $d_{S2}/\xi_n \gg 1$ and $\gamma_B^{-1} \gg 1$, we obtain the parameter of the S_2F_1 interface

$$\beta_\varepsilon = \frac{1}{\gamma_B^F}\frac{\varsigma}{d_{S2}\xi_n}\frac{\sigma_1^F}{\sigma_2}, \tag{19}$$

where $\varsigma \simeq 1$. Substituting Eq. (19) into Eq. (11), we find the sought pair-breaking rate γ_0.

The above formulas are used to study the critical parameters of the S_2 layer and the Josephson current in the acceptor junction versus the combined influence of the proximity effect with the ferromagnetic layer F_1 on one hand, and tunneling injection of nonequilibrium excitations on the other hand. In addition, the nonequilibrium effects due to the reabsorption of phonons can also affect the superconductivity of the S_1 layer, where the proximity-induced magnetization is negligible. Therefore, the present model includes the proximity effect between the S_2 and F_1

layers, whereas the change of superconductivity owing to the nonequilibrium tunneling injection is considered in both the S_1 and S_2 layers.

Depending on the intensity of the quasiparticle injection, one can define two regimes of the nonequilibrium state, characterized by two different instabilities [13]. These are created by two different types of the nonequilibrium sources, which are distinguished by a parameter $\tilde{\delta} = (V_i - 2\Delta)/2\Delta$, where V_i is the bias voltage across the injector. One is the so-called *threshold* instability, realized in the "narrow-band" source regime for which $\tilde{\delta} \ll 1$, while the other is realized in the "broadband" source regime, for which $\tilde{\delta} \gg 1$. Both types of instabilities will be discussed below. In our particular experiment (see the black squares and red circles in Fig. 4), a strong suppression of the acceptor critical supercurrent occurs when the bias voltage across the injector reaches $V_i = V_{\rm th}^b \approx 3.5$ mV, which, according to Ref. [13], corresponds to the "broad" source of nonequilibrium injection. Therefore, in the current experimental system, the injector represents a "broad" source of quasiparticles, characterized by a "threshold" voltage $V_{\rm th}^b$ (see $I-V$ curves of the injector junction reported in Fig. 5 of Ref. [31]). In the experiment, the magnitude of $V_{\rm th}^b$ depends on the device parameters and corresponds to the values of V_i at which both $\Delta_{1,2}(\beta_\varepsilon)$ and critical current $I_{\rm ca}$ are strongly suppressed, but remain finite. In our theoretical model, for the sake of convenience, we define $V_{\rm th}^b$ as being equal to the values of V_i at which both $\Delta_{1,2}(\beta_\varepsilon)$ and $I_{\rm ca}$ vanish. By biasing the injector junction up to a sufficiently high voltage $V_i \geq V_{\rm th}^b$, one can control the superconducting state by creating the nonequilibrium conditions. In particular, exceeding a critical concentration of the injected quasiparticles at $V_i \geq V_{\rm th}^b$ results in *switching* of the acceptor junction into the resistive state (in a practical situation, the acceptor could be prebiased at some current below $I_{\rm ca}$; a current pulse arriving at the injector junction would switch the acceptor junction into the resistive state). The model assumptions about the broad and narrow injection sources make the problem solvable analytically, which is very useful for critical analysis and modeling of the complex system under consideration. In Secs. 5 and 6 of the Appendix we describe the numeric procedure that allows us to compute $V_{\rm th}^b$ versus parameters of the hybrid multilayered device.

Using the pair-breaking rate approximation, we obtain the critical Josephson current of the acceptor in the form

$$I_{\rm ca} = \frac{\sigma_2 \Delta_1(V_i)\Delta_2(V_i)}{2e\xi_2\gamma_B}\,{\rm Re}\int_{-\infty}^{\infty}\frac{1}{\zeta_1(\varepsilon,V_i)}\frac{1}{\zeta_2(\varepsilon,V_i)} \times (1 - f_\varepsilon^{(1)} - f_\varepsilon^{(2)})d\varepsilon, \quad (20)$$

where $f_\varepsilon^{(1,2)}$ are the nonequilibrium electron distribution functions in the $S_{1,2}$ layers, $\zeta_1(\varepsilon, V) = \sqrt{\varepsilon^2 - \Delta_1^2(V_i)}$, $\Delta_{1,2}(V_i)$ are the superconducting energy gap in the $S_{1,2}$ layers, and

$$\zeta_2(\varepsilon, V_i) = \sqrt{\varepsilon^2 - \left[\Delta_2(V_i) - \alpha_2\frac{\zeta_\varepsilon^2}{\Delta_2(V_i)}\right]^2}; \quad (21)$$

where

$$\alpha_2 = \frac{\sigma_1^F}{\sigma_2}\frac{d_{S2}}{\xi_n}\frac{1}{2\gamma_B}, \quad (22)$$

with σ_1^F and σ_2 the electric conductivities of the ferromagnetic layer F_1 and the superconducting layer S_2, respectively. Equations (20) and (21) describe the nonequilibrium proximity effect, acting between the superconducting and ferromagnetic layers under the condition of quasiparticle injection; its influence on the Josephson current of acceptor junction has, to our knowledge, not been discussed previously in the literature.

In Eqs. (20) and (21), both the energy gaps $\Delta_1(V_i)$ and $\Delta_2(V_i)$ in the S_1 and S_2 layers explicitly depend on the bias voltage V_i across the injector. This dependence originates from nonequilibrium effects caused by tunneling of quasiparticle excitations supplied from the injector according to Fig. 1. Under the conditions of our experiment, the injector represents a broad source with a threshold voltage $V_{\rm th}^b \approx 3.5$ mV supplying the nonequilibrium quasiparticles into the S_1IS_2 junction (see Fig. 1). The injected quasiparticles fill empty electron states in its electrodes, thereby weakening the Cooper coupling and inhibiting the phase-coherent correlations. This results in suppression of the superconducting gaps $\Delta_{1(2)}(V_i)$ and the critical supercurrent $I_{\rm ca}(V_i)$ of the acceptor. Therefore, by creating the nonequilibrium conditions we control the superconducting state by changing the magnitudes of $\Delta_{1(2)}(V_i)$.

In the absence of the proximity effect between S and F, the nonequilibrium suppression of the superconductivity in a tunnel junction has been considered previously in the literature [13,15–19]. In the present work, we use a similar approach based on the Boltzmann equation for the nonequilibrium distribution function $f_\varepsilon^{(1,2)}$ [28–30] in the $S_{1,2}$ layers, in order to describe the proximity effect in an SF bilayer under nonequilibrium conditions.

IV. NONEQUILIBRIUM SUPPRESSION OF THE SUPERCONDUCTING CORRELATIONS IN HYBRID MULTILAYERS

The calculated results for $\Delta_2(V_i)$ are shown in Fig. 2(a), where we assume that the nonequilibrium source is "broad" [i.e., considerable suppression of Δ_2 occurs when the injector junction is biased at a voltage considerably larger than $V_i = (\Delta_2 + \Delta_3)/e$; this case is realized in our experiment]. The dependence of $\Delta_1(V_i)$ is similar to $\Delta_2(V_i)$, but

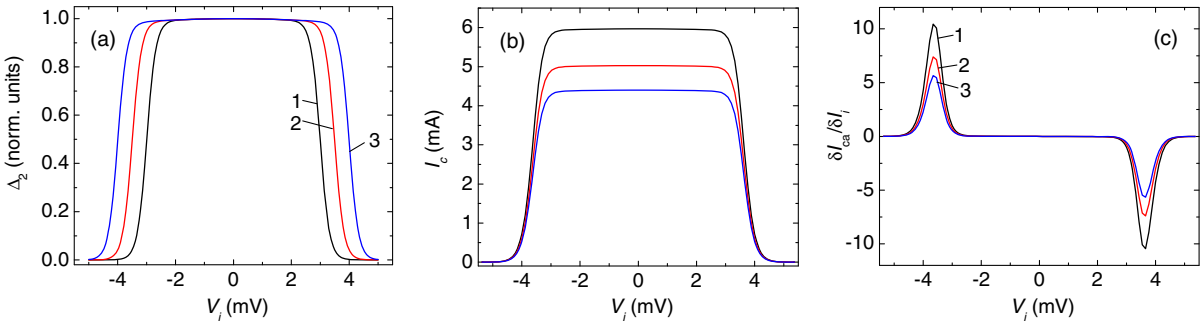

FIG. 2. (a) The dependence of the superconducting energy gap Δ_2 versus the bias voltage V_i applied across the $S_2F_1IF_2S_3$ injector junction for different magnitudes of the threshold voltage $V_{\rm th}^b$. Curves 1 to 3 correspond to $V_{\rm th}^b = 3$ mV, 3.5 mV, and 4 mV, respectively. (b) Suppression of the critical current of the $S_1I_1S_2F_1$ acceptor junction versus V_i for different values of the pair-breaking parameter $\alpha_V = 0.025$, 0.8, and 1.2 (curves from top to bottom, respectively). The critical current $I_{\rm ca}(V_i)$ drops abruptly when the bias voltage across the injector reaches its threshold value $V_i = V_{\rm th}^b \approx 3.5$ mV. (c) The small-signal gain $\delta I_{\rm ca}/\delta I_i$ versus the bias voltage V_i for different phonon escape rates $\gamma_{\rm ph}$. Curves from 1 to 3 correspond to $\gamma_{\rm ph} = 0.05\Delta$, 0.15Δ, and 0.3Δ, respectively. Junction parameters are given in the text.

the magnitude of Δ_1 is larger, $\Delta_1 > \Delta_2$. One can conclude from the $\Delta_2(V_i)$ plot that the superconducting energy gap in the S_2 layer of acceptor region is abruptly suppressed after the bias voltage V_i exceeds a threshold value $V_{\rm th}^b \approx 3$–4 mV. Furthermore, from Eq. (20) one can immediately see that the Josephson current of the acceptor junction is sensitive not only to the $\Delta_2(V_i)$ dependence, but also explicitly depends on the shape of $f_\varepsilon^{(1,2)}$ obtained by solving the Boltzmann equation discussed in Secs. 4–6 of the Appendix. Similar Boltzmann equations had been derived and solved in a number of studies (see, e.g., Refs. [13,17,18,20], and references therein). The $S_1I_1S_2$ interface transparency Υ_B (i.e., the acceptor junction transparency), enters via γ_B [see Eq. (5)]. For the particular conditions of our experiment, the nonequilibrium distribution function $f_\varepsilon^{(1,2)}$ allows us to write the critical Josephson current in a tractable form

$$I_{\rm ca} = \frac{\sigma_2}{2e\xi_2\gamma_B}\frac{2\Delta_1(V_i)\Delta_2(V_i)}{i(\alpha_2 - i)\chi_V} \times F\left(\csc^{-1}\left(\frac{\Delta_1}{\chi_V}\right)\middle|\frac{(2i\alpha_2+1)}{(\alpha_2-i)^2}\frac{\Delta_1^2}{\chi_V^2}\right), \quad (23)$$

where $\chi_V = \sqrt{\Delta_1^2(V_i) - \Delta_2^2(V_i)}$, $\csc^{-1}(z)$ involves the complex number z, $F(\varphi|m)$ is the elliptic integral of the first kind, and α_2 is defined by Eq. (22). Equation (23) has been obtained by approximating the electron distribution functions as $f_\varepsilon^{(1,2)} = f_\varepsilon^F + \delta f_\varepsilon$ with $\delta f_\varepsilon = f_0\Gamma_e/[(\varepsilon-\Delta)^2 + \Gamma_e^2]$; the magnitude f_0 and width Γ_e are computed by solving the Boltzmann equation as described in Appendix (see Secs. 4–6).

The $I_{\rm ca}(V_i)$ dependence calculated according to Eq. (20) is shown in Fig. 2(b). Here, $I_{\rm ca}$ is the critical Josephson current through the $S_1I_1S_2F_1$ acceptor junction, and V_i is the bias voltage applied across the $S_2F_1IF_2S_3$ injector junction. For the calculations we use experimental parameters for one of our devices as follows: the normal-state specific tunnel resistance of the injector $R_{T(i)} = 1.7\ \mu\Omega{\rm cm}^2$; injector area $A_i = 8\times 6\ \mu{\rm m}^2$; and the corresponding parameters for the acceptor $R_{T(a)} = 0.15\ \mu\Omega\,{\rm cm}^2$ and $A_{\rm i} = 8\times 8.5\ \mu{\rm m}^2$. The device has a 42-nm-thick S_2 (Nb) layer, a 2.7-nm-thick F_1 (Ni) layer, and a 6.7-nm-thick F_2 (Ni) layer. One can see from Fig. 2(b) that $I_{\rm ca}(V_i)$ sharply drops to zero after the bias voltage on the injector exceeds the threshold value $V_{\rm th}^b \approx 3.5$ mV. Such a sudden drop of the acceptor critical current is caused by two factors: (i) the immediate suppression of $I_{\rm ca}$ due to excessive population of the electron states by the nonequilibrium quasiparticles that tunnel from the injector, and (ii) the suppression of the superconductivity in the whole acceptor region, representing a dominant effect. Figure 2(c) shows the "small-signal" gain $\delta I_{\rm ca}/\delta I_i$ versus the bias voltage V_i for different phonon escape rates $\gamma_{\rm ph}$, characterizing the loss of phonons from the film into the substrate. The nonequilibrium part δN_ω of the phonon distribution function $N_\omega = N_\omega^{(0)} + \delta N_\omega$ [where $N_\omega^{(0)} = 1/(\exp(\omega/T) - 1)$] has a narrow maximum at $\omega = 2\Delta$ (see Refs. [13,28,30]), and is analytically approximated as $\delta N_\omega = N_0\gamma_{\rm eff}/[(\omega - 2\Delta)^2 + \gamma_{\rm eff}^2]$, where $\gamma_{\rm eff} = \gamma_{\rm PE} + \gamma_{\rm PX}$ is an effective width of δN_ω, $\gamma_{\rm PE} = \hbar/\tau_{\rm PE} \simeq 0.2$ meV is the phonon-electron relaxation rate, $\tau_{\rm PE}$ is the phonon-electron relaxation time, $\gamma_{\rm PX} = \hbar/\tau_{\rm PX}$, where for our setup the phonon escape time is about $\tau_{\rm PX} = 10^{-11}$ s, and we use $N_0 = 0.3N_\omega^{(0)}$.

The numerically computed dependence of the threshold voltage $V_{\rm th}$ versus $R_{T(i)}/R_{T(a)}$ is shown in Fig. 3. The influence of the nonequilibrium injection on the critical current of the acceptor, which is determined by the magnitude of the energy gap $\Delta_{1,2}$ of the $S_{1,2}$ layers, is described by the self-consistency equation (A36). The dependence of the threshold voltage $V_{\rm th}$ versus the ratio

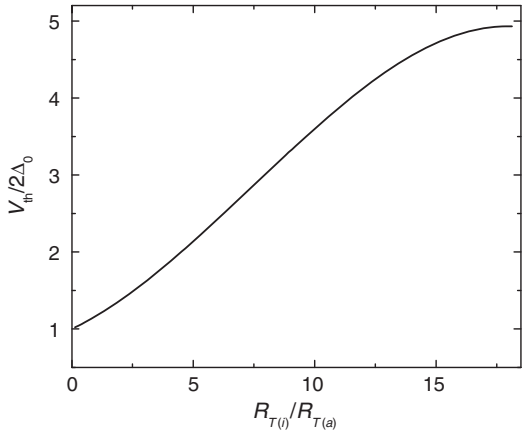

FIG. 3. Dependence of the threshold voltage $V_{\rm th}$ versus $R_{T(i)}/R_{T(a)}$ for $k_BT = 0.7\Delta$.

of the injector and acceptor resistances $V_{\rm th}(R_{T(i)}/R_{T(a)})$ is computed solving the self-consistency equation (A36). To deduce the dependence $V_{\rm th}(R_{T(i)}/R_{T(a)})$ for arbitrary $R_{T(i)}/R_{T(a)}$, which encompasses both the narrow and broad sources, we have used the nonequilibrium electron distribution function f_ε obtained by solving the Boltzmann equation (A19) numerically as described in Secs. 5 and 6 of the Appendix. As a zero-order input for the iterative scheme we use the relaxation time approximation (RTA) expression (A35). The numeric solutions obtained of Eq. (A36) determine the threshold instability, occurring at certain values of V_i, corresponding to $V_{\rm th}$ at which $\Delta_{1,2}$ vanish; the magnitude of V_i depends on the resistance of the injector $R_{T(i)}$, and the thicknesses of the $S_{1,2}$ layers, provided that all the other parameters of the device are fixed.

The model described is used for fitting the experimental $I_{\rm ca}(I_i)$ dependence measured at 4.2 K for the hybrid

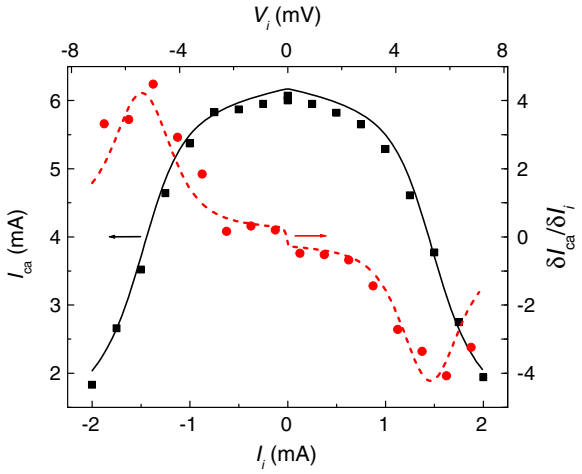

FIG. 4. Theoretical (black solid line) and experimental (black squares) dependence of the critical current of the acceptor $I_{\rm ca}$ versus the injection current I_i. The red dashed line and red circles show the corresponding dependence of the gain $\delta I_{\rm ca}/\delta I_i$.

multilayered $Nb_{(1)}/Al/AlO_x/Nb_{(2)}/Ni_{(1)}/Al/AlO_x/Ni_{(2)}/Nb_{(3)}$ three-terminal SFT devices [31] (see Fig. 4). The Josephson critical current density of the acceptor junction in the particular experimental device is 8.9 kA/cm^2, and the ratio of the specific tunneling resistances for the injector and acceptor junctions $R_{T(i)}/R_{T(a)} = 11.6$. The experimental $I_{\rm ca}$ versus I_i dependence is deduced from the $I_{\rm ca}(H)$ dependences taken at different levels of the injection current I_i; the squares in Fig. 4 correspond to maximum values of $I_{\rm ca}$ in the $I_{\rm ca}(H)$ dependences (such $I_{\rm ca}$ values do not necessarily correspond to $I_{\rm ca}$ at $H = 0$). The maximum small-signal current gain, $\delta I_{\rm ca}/\delta I_i$, observed for this device, is 4. These experimental data are used to compute the theoretical dependences. Black squares and the black line in Fig. 4 show, respectively, experimental and theoretical dependences of the critical current of the acceptor $I_{\rm ca}$ versus injection current I_i. The red dashed line and the red circles show corresponding dependence of the gain $\delta I_{\rm ca}/\delta I_i$. Note the relatively good agreement between the experimental data and the theory.

V. STRATEGIES FOR IMPROVING THE GAIN

There are several possible strategies to improve the gain of the SFT devices. Two of these involve the nonequilibrium effects caused by quasiparticle injection, and the influence of the proximity effect in the S_2F_1 sandwich. In addressing these it is important to maintain a high value of the steady-state critical supercurrent $I_{\rm ca}$ of the acceptor, which is diminished owing to the inverse proximity effect between the S_2 and F_2 layers.

Along with a straightforward increase of the magnitude of $I_{\rm ca}$, which is accomplished by increasing the acceptor transparency Υ_B (in the experiment we can increase Υ_B by a factor of 2.5, or even more), the gain can also be improved by a proper tuning of the balance between the nonequilibrium effects on one hand, and the proximity effect in the S_2F_1 bilayer on the other. According to the plots in Fig. 4, the slope of the $I_{\rm ca}(V_i)$ curve at the injector bias voltage $V_i = V_{\rm th}^b$ determines the gain of the hybrid multilayer. Physically, the slope of the $I_{\rm ca}(V_i)$ curve for the hybrid multilayered device [see Figs. 2(b) and 4] is mostly governed by the excess population of the nonequilibrium quasiparticles which are injected into the S_2 layer (see Fig. 1). This excess population causes a drastic suppression of the superconducting correlations in the acceptor region, which in turn suppresses the critical current $I_{\rm ca}$ of the acceptor. Therefore, in order to achieve the highest gain, the current-induced suppression of the superconductivity in the S_1 and S_2 layers must be made as sharp as possible.

It follows from some theoretical estimates [15] and from the experiment [31] that the gain of the double-barrier quasiparticle-injection devices is higher if the transparency of the acceptor junction Υ_B is higher than that of the injector junction $\Upsilon_{\rm inj}$. This is illustrated in Fig. 5, where we

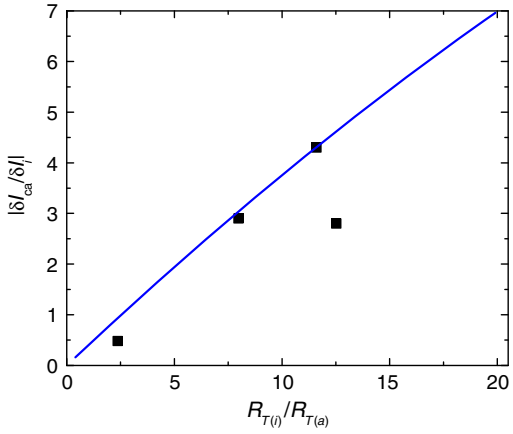

FIG. 5. Dependence of the gain $|\delta I_{\rm ca}/\delta I_i|$ versus the ratio of specific tunneling resistances of the injector $R_{T(i)}$ and acceptor $R_{T(a)}$ junctions in units of $R_{T(i)}/R^{\rm max}_{T(a)}$ with $R^{\rm max}_{T(a)} = 1.7\ \mu\Omega\,{\rm cm}^2$. Squares, experimental data for four different devices; blue line, theoretical fit. See text for details.

compare the experimental dependence of maximum gain $|\delta I_{\rm ca}/\delta I_i|$ versus $R_{T(i)}/R_{T(a)}$ obtained for four devices (squares) with the theoretically calculated dependence using the model developed here (shown as the line). The experimental data are obtained by averaging the gain values for two opposite directions of the injector current I_i. The theoretical curve is obtained using a fixed normal-state specific tunnel resistance of the injector of $R_{T(i)} = 1.7\ \mu\Omega\,{\rm cm}^2$, an injector area of $A_i = 8\times 6\ \mu{\rm m}^2$, and an acceptor area of $A_i = 8\times 8.5\ \mu{\rm m}^2$. The acceptor specific tunnel resistance $R_{T(a)}$ is varied between 0.085 and 1.7 $\mu\Omega\,{\rm cm}^2$.

The nonequilibrium effects in the acceptor region are enhanced when the quasiparticle-injection rate from an external source (i.e., the injector junction in our device) is increased, and simultaneously, the energy drain from the S_2 layer into the outside environment is decreased. A narrow-band source injects quasiparticles in a narrow energy interval $V_i - 2\Delta \ll 2\Delta$, so that the quasiparticles appear localized near $\varepsilon \sim \Delta$. The localized nature of the electron distribution function f_ε allows for defining a universal relation between Δ and the concentration of nonequilibrium quasiparticles $\bar{f}_\varepsilon = \int_0^\infty g(\varepsilon) f_\varepsilon d\varepsilon$, where $g(\varepsilon)$ is the electron density of states. Low energies $\varepsilon \sim \Delta_{1,2}$ of electron excitations cause the main contribution to Eq. (3), thereby determining steepness of the $\Delta_{1,2}(V_i)$ dependence. In the stability of the then on equilibrium state, created by a "narrow source" of quasiparticle excitations with energies $\varepsilon \sim \Delta_{1,2}$, is described using the Boltzmann equation [13]. The model of a narrow-band source is simplified by taking into account the fact that the relaxation processes due to the inelastic electron-phonon collisions are strongly suppressed in comparison with recombination processes. For sufficiently low temperatures $T \ll \Delta/k_B$, the solution of the Boltzmann equation can be obtained analytically [13]. Here, we use an analytical expression [13] for the electron distribution function:

$$f_z = A_V \frac{\sqrt{z}\theta(z)\theta(1-z)}{\sqrt{z(1-z)} + A_V(\sqrt{z}+\sqrt{1-z})}, \qquad (24)$$

where $\theta(z)$ is the Heaviside step function. The coefficient A_V in Eq. (24) satisfies the following normalization condition:

$$A_V^2 \int_0^1 \frac{dz}{\sqrt{z(1-z)} + A_V(\sqrt{z}+\sqrt{1-z})} = \frac{\alpha_V}{4\sqrt{\tilde{\delta}}}, \qquad (25)$$

where

$$z = \frac{\varepsilon-\Delta}{\Delta\tilde{\delta}} = 2\frac{\varepsilon-\Delta}{V_i-2\Delta}, \qquad \tilde{\delta} = \frac{V_i-2\Delta}{2\Delta},$$
$$f_z = f(z), \qquad \alpha_V = \frac{2\sigma_{\rm inj}\tau_{\rm EP}}{d_{S2}e^2 g(0)}, \qquad (26)$$

$\tau_{\rm EP}$ is the electron-phonon relaxation time (see Sec. 4 of the Appendix), d_{S2} is the thickness of the S_2 layer, and $g(0)$ is the electron density of states at the Fermi level; the layer indices are omitted in Eq. (26). The injector conductivity $\sigma_{\rm inj}$, which enters Eq. (26), is

$$\sigma_{\rm inj} = \sigma_0 \Upsilon_{\rm inj}, \qquad (27)$$

where $\sigma_0 = 2e^2 g_2(0) v_{F2}$, and the effective transparency of the injector $\Upsilon_{\rm inj}$ is computed in Sec. 4 of the Appendix. Knowledge of the nonequilibrium electron distribution function f_z given by Eq. (24) allows us to compute the gain $\delta I_{\rm ca}/\delta I_i$ of the hybrid SFT device for a narrow-source operation mode.

In our experimental device, the injector works as a broad nonequilibrium quasiparticle source (for which $V^b_{\rm th} > 2\Delta_{1,2}/e$), which is not optimal for achieving the maximal gain. According to our calculations, considerably higher gains can be achieved in the narrow-source mode of operation, which requires the threshold voltage $V^n_{\rm th}$ to be close to the gap-sum voltage. The nonequilibrium instability mechanisms for the broad and narrow sources are different from each other, and are described using different models [13]. Therefore, the voltage dependences of the energy gaps $\Delta_{1,2}(V_i)$ versus the bias voltage V_i across the injector are different for the two cases, and generally $V^n_{\rm th} \neq V^b_{\rm th}$, $V^n_{\rm th} \ll V^b_{\rm th}$. A straightforward way to make $V^n_{\rm th}$ lower is to increase the injector transparency $\Upsilon_{\rm inj}$, computed in Secs. 4–6 of the Appendix. This is illustrated in Fig 6. Figure 6(a) shows the calculated energy gap Δ_2 of the S_2 layer (normalized to its value at $I_i = 0$) versus the injector current I_i, and the corresponding current gain, $|\delta I_{\rm ca}/\delta I_i|(I_{\rm i})$. The parameters of the device used to

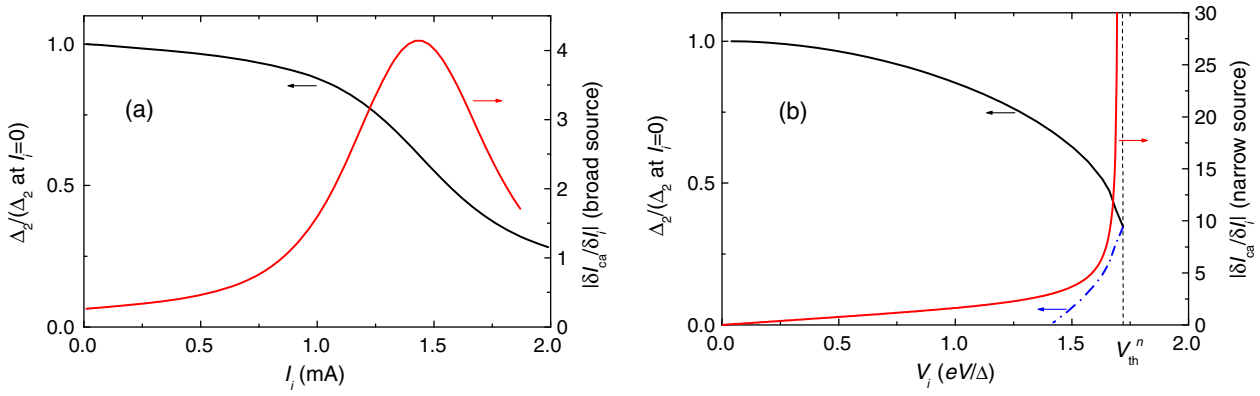

FIG. 6. (a) The dependence of the normalized energy gap Δ_2 in the S_2 layer and the corresponding gain $|\delta I_{ca}/\delta I_i|$, versus the bias current through the injector for the broad source. (b) The same gap versus the bias voltage across the injector for the narrow source.

calculate these dependences are taken from the experiment (cf. Fig. 4). One obtains a maximum gain of about 4.

For a projected device working in the narrow-source regime, a much higher current gain can be obtained [see Fig. 6(b)]. In this figure, we plot the energy gap Δ_2 and the corresponding gain $|\delta I_{ca}/\delta I_i|$ versus the normalized bias voltage V_i. The gain rapidly grows when V_i approaches the back-bending point of the $\Delta_2(V_i)$ dependence.

The $\Delta_2(V_i)$ dependence is analytically deduced using the self-consistency equation (3) for the energy gap, from which one obtains [13]

$$\Delta_2^{(0,\pm)} = \left[0, \frac{\varphi}{2\alpha}\left(1 \pm \sqrt{1 - \frac{4\alpha\delta}{\varphi^2}}\right)\right]. \tag{28}$$

In Eq. (28), $\alpha \simeq 1$, $\delta = (a - a_c)/a_c$,

$$a = \int_{\Delta_2}^{\infty} f_\varepsilon^{(0)} \frac{\varepsilon}{\varepsilon^2 - \Delta_2^2} d\varepsilon; \qquad a_c = \int_0^{\infty} f_\varepsilon^{(0)} \frac{d\varepsilon}{\varepsilon}, \tag{29}$$

and φ is a measure of nonequilibrium effect

$$\varphi = \frac{\pi}{a}\int_{\Delta_2}^{\infty} [f_\varepsilon f_{\Delta_2} - N_{\varepsilon+\Delta_2}(1 - f_\varepsilon - f_{\Delta_2})] \frac{d\varepsilon}{\sqrt{\varepsilon^2 - \Delta_2^2}}, \tag{30}$$

where N_ω is the phonon distribution function, which should be obtained from a corresponding Boltzmann equation for phonons; however, here we use an approximation $N_\omega \approx N_\omega^{(0)}$, where $N_\omega^{(0)} = 1/(e^{\omega/k_BT} - 1)$. In the limiting case $\varepsilon - \Delta_2 \ll \Delta_2$ and $N_{\varepsilon+\Delta} \simeq 0$, one finds $\varphi \simeq (\pi/2\Delta_2^{(0)})\ln(\Delta_2^{(0)}/\Delta_2)$, where $\Delta_2^{(0)}$ is the steady-state energy gap in the absence of injection. Mathematically, Eq. (28) is a nonlinear equation in $\Delta_2(V_i)$ provided that the above conditions are observed. The $\pm$ signs in Eq. (28) correspond to an increase or decrease of $\Delta_2(V_i)$ near the threshold bias voltage $V_i = V_{th}^n$ matching the threshold value of the pumped power W_{th}^n achieved when $\Delta(V_i)$ sharply decreases. From Fig. 6(a) one can see that the broad-source case corresponds to a fairly gradual change of $\Delta_2(V_i)$.

For the narrow source, when the bias voltage on the injector is in the range $1.4\Delta/e < V_i < V_{th}^n$, multiple values of the energy gap $\Delta_{0,\pm}$ occur in the S_2 layer [see Fig. 6(b)] (28). The lower Δ_- branch of $\Delta(V_i)$ [see the blue dash-doted line in Fig. 6(b)] is *unstable*, while the upper Δ_0 and Δ_+ branches are *metastable*. According to general properties of the Boltzmann equation for f_ε, the whole system experiences a transition from an initial state with Δ_+ into the another state with $\Delta_0 \equiv 0$. In the absence of large fluctuations, the switching to the resistive state takes place when V_i reaches V_{th}^n.

The gain $\delta I_{ca}/\delta I_i$ is determined by the coupling energy δ between the acceptor and injector [34,35], which is defined as a difference between the Josephson energy E_{ia} [36] of the whole multilayered structure (involving the injector and acceptor) and the sum of Josephson energies $E_i + E_a$ of the noninteracting injector (i) and acceptor (a) junctions. In this case, the maximum gain magnitude is obtained when δ is minimized. By decreasing the thickness of the S_2 layer from 30–45 nm (in the present experimental devices) down to 8–10 nm, and simultaneously increasing the acceptor transparency Υ_B by a factor of 3 or so (i.e., from the present junction transparency $\Upsilon_B = 8.5 \times 10^{-6}$ to a higher transparency $\Upsilon_B = 2.5 \times 10^{-5}$), one can obtain the coupling $\delta \sim 10^{-2}\Delta$, which yields $\delta I_{ca}/\delta I_i \simeq \Delta/\delta \sim 10^2$.

A qualitative picture of the threshold instability taking place in the narrow-source regime is as follows. Assume that initially $\Delta(V_i) = \Delta_+$ [upper branch; solid black curve in Fig. 6(a)], and $V_i \ll 2\Delta_+$. Then, fluctuations of the nonequilibrium quasiparticle concentration $\bar{f} = \int g(\varepsilon) f_\varepsilon d\varepsilon$ [here $g(\varepsilon)$ is the tunneling density of electron states] lead to a decrease in $\Delta(V_i)$ and, therefore, to an increase in the width of the source, proportional to $V_i - 2\Delta(V_i)$, which in turn increases $\bar{f}$, and so on.

Another way to improve the gain follows from our theoretical model, which suggests that the gain of the SFT device can be improved from ∼6 [see blue curve 3 in Fig. 2(c) corresponding to $\gamma_{\rm ph} = 0.3\Delta$] to ∼11 [black curve 1 in the same Fig. 2(c) corresponding to $\gamma_{\rm ph} = 0.05\Delta$]; this can be accomplished, e.g., by inserting a thin metal film with a different acoustic impedance [37] beneath the hybrid multilayer.

Further enhancement of the nonequilibrium effects and reduction of the threshold voltage can be realized by decreasing the thickness d_{S2} of the S_2 layer, thereby increasing the energy density pumped by the injector into the S_2 layer. Assuming that the nonequilibrium distribution function remains homogeneous inside the S_2 film, we represent the absorbed power threshold $W_{\rm th}$ as $W_{\rm th} \propto \beta_{\rm th}(T) d_{S2}$, which suggests that $W_{\rm th}$ can be decreased by using thinner films with smaller d_{S2}. For instance, a threefold reduction of the thickness d_{S2} of the S_2 layer gives a threefold reduction in the threshold power, which enables the injector to work in the narrow nonequilibrium source regime.

VI. CONCLUSIONS

We have formulated a tractable analytical model of a multilayered superconductor-ferromagnetic structure which functions as a superconducting-ferromagnetic transistor, whose superconducting properties and phase-coherent transport are controlled by the tunneling injection of nonequilibrium quasiparticles. In addition to the tunneling injection, the proximity effect between the superconducting and magnetic layer is also responsible for suppression of the superconductivity in the middle electrode shared by the injector and acceptor junctions. The second factor depends on the interface transparencies, which are closely related to the magnitude of the pair-breaking rate.

The combined influence of the inverse proximity effect between the superconducting and ferromagnetic layers, on one hand, and nonequilibrium quasiparticle injection on the other, may result in a high amplification factor $\delta I_{\rm ca}/\delta I_i$. The proposed theoretical model establishes a physical framework for optimization of the device performance.

Detailed comparison of the calculated values for the suppression of the superconducting correlations in the acceptor with the corresponding experimental data obtained for our SFT devices shows good agreement between the experiment and the model. A remarkable result for the narrow-source regime is that the dependence of the energy gap in the S_2 layer versus the bias voltage across the $S_2F_1I_2F_2S_3$ injector becomes much steeper when approaching the threshold voltage $V_{\rm th}$. We expect that in this case the current gain $\delta I_{\rm ca}/\delta I_i$ can be improved by approximately 2 orders of magnitude as compared to the value obtained for the broad nonequilibrium source regime. Therefore, we conclude that multilayered superconductor-ferromagnetic devices have great potential for applications in the next-generation energy-efficient digital and memory circuits.

ACKNOWLEDGMENTS

The research is based upon work supported by the Office of the Director of National Intelligence (ODNI), Intelligence Advanced Research Projects Activity (IARPA), via Raytheon Inc. Contract No. W911NF-14-C-0089. The authors acknowledge technical assistance rendered by Dr. O. Chernyashevskyy, valuable remarks by S. Holmes, useful discussions with I. Vernik, and encouragement from M. Manheimer and T. Ohki.

APPENDIX SUPPLEMENTAL INFORMATION

1. Basic equations

The Usadel equation for the pair amplitude versus coordinate x perpendicular to layers is derived using the Keldysh technique. The basic equations are obtained for the quasiclassical functions integrated over the electron kinetic energy. Since we consider a nonequilibrium system, we use a Keldysh framework of the quasiclassical theory, where the fundamental quantity is the momentum average of the quasiclassical Green's function $G(x,\varepsilon) = \langle G(\mathbf{p_F}, x, \varepsilon)\rangle_{\mathbf{p_F}}$. Here, x is the coordinate normal to the S/F interfaces and ε is a quasiparticle energy, and $\langle \ldots \rangle_{\mathbf{p}_F}$ means averaging over directions of the electron momentum. The reduction to the "dirty" limit is performed for the Keldysh Green's functions. The Usadel equation in the 4×4 Keldysh-Nambu space reads

$$D\check{\partial}_x\{\check{G}(\varepsilon,x)[\check{\partial}_x\check{G}(\varepsilon,x)]\} = [-i\varepsilon\check{\tau}_3 + \check{\Delta} + \check{\Sigma}, \check{G}(\varepsilon,x)], \tag{A1}$$

where $[A,B] = AB - BA$ and the product means a convolution in the nonstationary case, which is reduced to a conventional product in the stationary nonequilibrium case and the self-energy $\check{\Sigma}$ takes into account the electron-phonon and electron-electron interactions. The matrix structure is as follows:

$$\check{G} = \begin{pmatrix} \hat{G}^R & \hat{G}^K \\ 0 & \hat{G}^A \end{pmatrix}, \qquad \hat{G} = \begin{pmatrix} G & F \\ F^\dagger & G^\dagger \end{pmatrix},$$
$$\check{\Sigma} = \begin{pmatrix} \hat{\Sigma}^R & \hat{\Sigma}^K \\ 0 & \hat{\Sigma}^A \end{pmatrix}, \tag{A2}$$

$$\tau_3 = \begin{pmatrix} \hat{\tau}_3 & 0 \\ 0 & \hat{\tau}_3 \end{pmatrix}, \quad \check{\Delta} = \begin{pmatrix} \hat{\Delta} & 0 \\ 0 & \hat{\Delta} \end{pmatrix}, \quad \hat{\Delta} = \begin{pmatrix} 0 & \Delta \\ \Delta^* & 0 \end{pmatrix}. \tag{A3}$$

Although the Keldysh technique also works for time-dependent systems, we consider the simplest case of a

stationary nonequilibrium problem. The normalization condition takes the form $\check{G}\check{G}=1$; in terms of the components it implies $\hat{G}^R\hat{G}^R=\hat{G}^A\hat{G}^A=1$, and $\hat{G}^R\hat{G}^K+\hat{G}^K\hat{G}^A=0$. The second relation means that $\hat{G}^K$ can be parametrized using the matrix "distribution function" $\hat{f}$ as

$$\hat{G}^K=\hat{G}^R\hat{f}-\hat{f}\hat{G}^A. \tag{A4}$$

From the retarded (i.e., upper left) component of the Keldysh-Usadel equation (A1) we obtain the Usadel equation in the form

$$D\hat{\partial}_x[\hat{G}^R(\hat{\partial}_x\hat{G}^R)]=[-i\varepsilon\hat{\tau}_3+\hat{\Delta}+\hat{\Sigma}^R,\hat{G}^R(\varepsilon,x)]. \tag{A5}$$

Instead of using the anomalous Green's function F^R, it is convenient to introduce the pair amplitude Φ using the relation $F^R=G^R\Phi/\varepsilon$. Then, from Eq. (A5) one arrives to Eq. (1) used to describe the proximity effect between the superconducting S_2 and ferromagnet F_1 layers in the S_2F_1 sandwich.

From the Keldysh component (i.e., upper right) of the Keldysh-Usadel equation (26), one obtains the Boltzmann equation for the distribution function in the matrix form $\hat{f}$

$$\begin{aligned}&D\{\nabla^2\hat{f}+(\hat{G}^R\nabla\hat{G}^R)\nabla\hat{f}-\nabla\hat{f}(\hat{G}^A\nabla\hat{G}^A)-\nabla[\hat{G}^R(\nabla\hat{f})\hat{G}^A]\}\\&-(\hat{G}^R[\hat{\Delta},\hat{f}]-[\hat{\Delta},\hat{f}]\hat{G}^A)+i\varepsilon(\hat{G}^R[\hat{f},\hat{\tau}_3]-[\hat{f},\hat{\tau}_3]\hat{G}^A)\\&=0.\end{aligned} \tag{A6}$$

We have used the property that $\hat{G}^{R(A)}$ satisfies the corresponding components of the Usadel equation. The Boltzmann equation has only two independent entries. Furthermore, since it is a linear equation, we can assume that $\hat{f}$ is diagonal

$$\hat{f}=\begin{pmatrix}1-2f_\varepsilon & 0\\ 0 & 1-2\bar{f}_\varepsilon\end{pmatrix}, \tag{A7}$$

where f_ε and $\bar{f}_\varepsilon=1-f_\varepsilon$ are the distribution functions for electrons and holes and the energy ε is measured from the chemical potential of the superconductor. For our nonequilibrium hybrid multilayer system, the solution of the Boltzmann equation is considered in Secs. IV–VI below.

2. Josephson current

The boundary conditions (6) allow for computing the Josephson current in the junctions of arbitrary transparency. Multiplying the second equation of Eqs. (6) by $G_2^R\Phi_2^*$ gives

$$\begin{aligned}&\xi_2\gamma_BG_2^R\Phi_2'=G_1^R(\Phi_1-\Phi_2)\\&[G_2^R]^2\Phi_2^*\Phi_2'=\frac{1}{\xi_2\gamma_B}(G_1^RG_2^R\Phi_1\Phi_2^*-G_1^RG_2^R\Phi_2\Phi_2^*)\end{aligned} \tag{A8}$$

and using the expression for the Josephson current (4) we get

$$\begin{aligned}I&=\frac{2\sigma_2\pi}{e}\mathrm{Im}\int_{-\infty}^{\infty}i\frac{[G_2^R]^2\Phi_2^*\Phi_2'}{\varepsilon^2}\frac{d\varepsilon}{4\pi}\\&=\frac{2\sigma_2\pi}{e}\frac{1}{\xi_2\gamma_B}\mathrm{Re}\int_{-\infty}^{\infty}(G_1^RG_2^R\Phi_1\Phi_2^*-G_1^RG_2^R\Phi_2\Phi_2^*)\frac{1}{\varepsilon^2}\frac{d\varepsilon}{4\pi}\\&=\frac{2\sigma_2\pi}{e}\frac{1}{\xi_2\gamma_B}\mathrm{Re}\int_{-\infty}^{\infty}\frac{G_1^RG_2^R\Phi_1\Phi_2^*}{\varepsilon^2}\frac{d\varepsilon}{4\pi},\end{aligned} \tag{A9}$$

where the second term $\propto\mathrm{Im}\Phi_2\Phi_2^*$ in the parentheses vanishes. For the anomalous retarded Green's function we use

$$F_2^R=G_2^R\frac{\Phi_2}{\varepsilon}=\frac{\Delta_2}{\zeta_\varepsilon}=\frac{\Delta_2}{\zeta_2}=\frac{\Delta_2}{\zeta_2^{(0)}(\varepsilon)}\left(1-\frac{\beta_\varepsilon}{2}x^2\right), \tag{A10}$$

where $\zeta_{1,2}^{(0)}(\varepsilon)=\sqrt{\varepsilon^2-\Delta_{1,2}^2}$ and

$$\zeta_{1,2}=\sqrt{\varepsilon^2-[\Delta_{1,2}+i\gamma_0]^2}; \tag{A11}$$

here [see Eqs. (8), (11), (16), and (19)] $\gamma_0=\alpha_2(\zeta_2)^2/\Delta_2$ and $\beta_\varepsilon=2\alpha_2/d_F^2$, where we assume that thicknesses of both the $F_{1,2}$ layers are the same and equal to d_F. We then find

$$\begin{aligned}I&=\frac{2\sigma_2\pi}{e\xi_2\gamma_B}\mathrm{Im}\int_{-\infty}^{\infty}i\frac{\Delta_1}{\zeta_1^{(0)}(\varepsilon)}\frac{\Delta_2}{\zeta_2(\varepsilon)}(1-f_\varepsilon-f_\varepsilon^F)\frac{d\varepsilon}{4\pi}\\&=\frac{\sigma_2\Delta_1\Delta_2}{2e\xi_2\gamma_B}\mathrm{Re}\int_{-\infty}^{\infty}\frac{1}{\zeta_1^{(0)}(\varepsilon)}\frac{1}{\zeta_2(\varepsilon)}(1-f_\varepsilon-f_\varepsilon^F)d\varepsilon,\end{aligned} \tag{A12}$$

where $\Delta_2=\Delta_2(V_\mathrm{i})$ depends on the injector bias voltage V_i, and f_ε is the nonequilibrium electron distribution function $f_\varepsilon^F=[\exp(\varepsilon/T)+1]^{-1}$. The suppression of the superconducting energy gap Δ_2 due to the inverse proximity effect between the superconducting S and ferromagnetic layers F is controlled by the parameter

$$\alpha_2=\beta_\omega\frac{d_F^2}{2}=\frac{1}{2\gamma_B}\frac{\sigma_1}{\sigma_2}\frac{d_{S2}}{\xi_n}, \tag{A13}$$

where d_{S2} is the thickness of the S_2 layer, γ_B is defined by Eq. (5), and $\sigma_{1,2}$ is the normal-state conductivity of the $S_{1,2}$

layer. For a symmetric Josephson junction (i.e., in the absence of nonequilibrium injection), at $T = 0$ one computes the integral explicitly

$$\int_{-\infty}^{\infty} \frac{\Delta^2}{\sqrt{\Delta^2+x^2}\sqrt{\left(\Delta+\alpha_2\frac{(\Delta^2+x^2)}{\Delta}\right)^2+x^2}}dx = \frac{2\Delta\alpha_2}{\alpha_2\sqrt{2\alpha_2+1}}\cot^{-1}\left(\frac{\alpha_2}{\sqrt{2\alpha_2+1}}\right). \tag{A14}$$

The dependence $\Delta(V_i)$ versus the bias voltage V_i is determined by the nonequilibrium injection from the SFIFS junction.

3. Nonsymmetric junction

The corresponding expression for a nonsymmetric case contains the integral

$$\begin{aligned} I_{\mathrm{NS}} &= \Delta_2\Delta_1\int_{-\infty}^{\infty}\frac{dx}{\sqrt{\Delta_1^2+x^2}\sqrt{x^2+\left(\Delta_2+\alpha_2\frac{(\Delta_2^2+x^2)}{\Delta_2}\right)^2}} \\ &= \frac{2\sqrt{\frac{\alpha_2^2}{(\alpha_2-i)^2}}F\left(\left.\frac{\csc^{-1}\left(\frac{\Delta_1}{\sqrt{\Delta_1^2-\Delta_2^2}}\right)\sqrt{1-\frac{\Delta_2^2}{\Delta_1^2}\Delta_1}}{\sqrt{\Delta_1^2-\Delta_2^2}}\right|\frac{(2i\alpha_2+1)\Delta_1^2}{(\alpha_2-i)^2(\Delta_2^2-\Delta_1^2)}\right)}{\Delta_1^2\sqrt{\frac{\Delta_2^2(\Delta_1^2-\Delta_2^2)}{\Delta_1^4}}\sqrt{-\frac{\alpha_2^2}{\Delta_2^2}}} \\ &= \frac{2\Delta_2\Delta_1}{i(\alpha_2-i)\sqrt{\Delta_1^2-\Delta_2^2}} \times F\left(\csc^{-1}\left(\frac{\Delta_1}{\sqrt{\Delta_1^2-\Delta_2^2}}\right)\middle|\middle|\frac{(2i\alpha_2+1)}{(\alpha_2-i)^2}\frac{\Delta_1^2}{\Delta_2^2-\Delta_1^2}\right), \end{aligned} \tag{A15}$$

where $\csc^{-1}(z)$ (or arccsc) gives the arc cosecant of the complex number z and $F(f|m)$ is the elliptic integral of the first kind. If pair breaking is energy independent, one can use a simpler formula

$$\Delta_1\Delta_2\int_{-\infty}^{\infty}\frac{d\omega}{\sqrt{(\omega^2+\Delta_1^2)(\omega^2+\Delta_2^2)}} = \frac{2\Delta_1\Delta_2}{\Delta_1+\Delta_2}K\left(\frac{|\Delta_1-\Delta_2|}{\Delta_1+\Delta_2}\right). \tag{A16}$$

The equilibrium critical Josephson current through the $S_1I_1S_2F_1$ junction is

$$I_c^{(0)} = \eta_M\frac{\Delta_1\Delta_2}{2\pi eR_{Na}}\int_{\max\{\Delta_1,\Delta_2\}}^{\infty}\frac{1}{\sqrt{\varepsilon^2-\Delta_1^2}}\frac{1}{\sqrt{\varepsilon^2-\Delta_2^2}} \times \tanh\frac{\varepsilon}{2T}d\varepsilon, \tag{A17}$$

where η_M takes into account the nonequilibrium effects. The last formula suggests that the Josephson critical current is affected by the change of Δ_2 due to a combined influence of the proximity with the F layer on one hand, and nonequilibrium change of Δ_2 on the other. In addition, there is a direct influence of the nonequilibrium tunneling injection on the value of I_c via the change of the electron distribution function, as discussed below. Under equilibrium conditions the Josephson current flowing between the two bulk superconductors at zero temperature is given by

$$I_c^{(0)} = \frac{\Delta_1\Delta_2}{eR_N}\int_{-\infty}^{\infty}\frac{d\omega}{\sqrt{(\omega^2+\Delta_1^2)(\omega^2+\Delta_2^2)}} = \frac{2\Delta_1\Delta_2}{eR_{Na}(\Delta_1+\Delta_2)}K\left(\frac{|\Delta_1-\Delta_2|}{\Delta_1+\Delta_2}\right), \tag{A18}$$

where $K(k)$ is the full elliptic integral of the first kind.

4. Tunneling injection of quasiparticles

The Boltzmann equation for the electron distribution function under the condition of the quasiparticle injection [13,15–19] is written as

$$\frac{\partial f_\varepsilon}{\partial t} = I_0\{H_+(f^F_{\varepsilon_+}-f_\varepsilon)+H_-(f^F_{\varepsilon_-}-f_\varepsilon) + \tilde{H}(1-f^F_{\tilde{\varepsilon}}-f_\varepsilon)\}+L_\varepsilon\{f_\varepsilon\}, \tag{A19}$$

where

$$H_\pm = \frac{\varepsilon_\pm\theta(\varepsilon_\pm-\Delta)}{\sqrt{\varepsilon_\pm^2-\Delta^2}}, \qquad \tilde{H} = \frac{\tilde{\varepsilon}\theta(\tilde{\varepsilon}-\Delta)}{\sqrt{\tilde{\varepsilon}^2-\Delta^2}}. \tag{A20}$$

Here, $\varepsilon_\pm = \varepsilon \pm eV_i$, $\tilde{\varepsilon} = eV_i-\varepsilon$, $f^F_\varepsilon = [\exp(\varepsilon/T)+1]^{-1}$, Δ and V_i are the gap and bias voltage of injector, and $L_\varepsilon\{f_\varepsilon\}$ is the electron-phonon collision integral, which in the simplest case is taken in the relaxation time approximation as

$$L_\varepsilon = -\frac{f_\varepsilon-f^F_\varepsilon}{\tau_{\mathrm{EP}}}, \tag{A21}$$

where τ_{EP} is the electron-phonon collision time [13,28–30]. A more general form of L_ε is considered in the next section. In Eq. (A19) the electron distribution function in the injector can be taken as the equilibrium one, but with shifted energy arguments. In this model, we disregarded the influence of the proximity effect on the electron-phonon collision time τ_{EP}, which is small when $\tau_{\mathrm{EP}}\delta\Delta_2 \ll 1$, where the change $\delta\Delta_2$ of the energy gap Δ_2 in the S_2 layer due to the proximity with the F_1 layer; $\delta\Delta_2$ is estimated using Eqs. (21) and (22) as $\delta\Delta_2 = \alpha_2\zeta_\varepsilon^2/\Delta_2 \simeq 0.25\Delta_2 \ll \Delta_2$. In the last formula, $\alpha_2 = \sigma_1^F d_{S2}/(2\gamma_B\sigma_2\xi_n) \ll 1$ since $\gamma_B = 2l_2(1-\Upsilon_2)/(3\xi_2\Upsilon_2) \gg 1$ and the transparency of the S_2F_1 interface is $\Upsilon_2 \ll 1$. The corrections to the energy

relaxation time due to the proximity effect are minor, since they change the energy dependence of it only slightly, which, nevertheless, remains slow on the energy scale of the superconducting gap. Therefore, the nonequilibrium and magnetization effects are nearly "decoupled" from each other and they have different impacts on the hybrid system. The Josephson current of the acceptor junction changes mostly due to deviation of f_ε from its equilibrium value f_ε^F. The role of the ferromagnetic layers is reduced to one of suppressing the superconducting correlations across the injector junction, whereas suppression of the superconductivity in the S_2 layer due to the inverse proximity effect with F_1 is minor and leads to a 25% reduction of Δ_2 in comparison with Δ_1. The time derivative on the left in Eq. (A19) is a generally accepted notation. It denotes collision terms, which are not given in explicit form, but which can appear in the Boltzmann equation in addition to the electron-phonon term. These include the electron-electron collisions, the diffusion of electrons along layers, etc. Typically those additional terms are much smaller than the terms describing the electron-phonon collision and tunneling injection. The tunneling injection parameter is

$$I_0 = \frac{2\Upsilon_{\rm inj} v_{F2}}{d_{S2}}, \tag{A22}$$

where v_{F2} is the Fermi velocity, d_{S2} is the thickness of the S_2 layer, and $\Upsilon_{\rm inj}$ is the effective transparency of injector. The parameter α_V in Eq. (26) is then $\alpha_V = I_0\tau_{\rm EP}$. The exact expression for $\Upsilon_{\rm inj}$ depends on details of the injector geometry and on the interface barriers. Practically, $\Upsilon_{\rm inj}$ is deduced from the experimental $I-V$ curve of the injector, while its microscopic calculation is conducted, e.g., using the S-matrix approach [38]. From Fig. 1 the injector has a multilayered $F_1I_2F_2I_3S_3$ geometry, where the ferromagnetic F_1 and F_2 layers are separated by the dielectric barrier I_2, while the F_2 and S_3 layers are separated by another interface barrier I_3, which is not shown in Fig. 1. Nevertheless, we introduce this additional barrier I_3 in the calculation below to take into account the finite transparency of the F_2S_3 interface, owing to difference of Fermi velocities in the F_2 and S_3 layers, and the imperfections of the interface. Therefore, the net transparency $\Upsilon_{\rm inj}$ of the whole $F_1I_2F_2I_3S_3$ multilayer is composed of partial transparencies of the component barriers and layers. We compute the transmission coefficient of the whole $F_1I_2F_2I_3S_3$ multilayer using the coherent approximation. For this we consider the whole injector setup shown in Fig. 1 as a composition $F_1I_2F_2I_3S_3 \rightarrow F_1I_2F_2 \odot I_2F_2I_3 \odot F_2I_3S_3$ of three consequent sections (each section of the whole setup is sketched in Fig. 1). The whole three-step composition $\hat{S}_{LR} = \hat{S}_L \odot \hat{S}_T \odot \hat{S}_R$ yields the net S matrix S_{LR} of the whole injector. Here, $\hat{S}_L$, $\hat{S}_T$, and $\hat{S}_R$ are the S matrices of the fractional $F_1I_2F_2$, $I_2F_2I_3$, and $F_2I_3S_3$ junctions, respectively, while L and T refer to the corresponding adjacent sections of the $F_1I_2F_2I_3S_3$ multilayer. The composition operator $\odot$ acts, e.g., as [38]

$$\hat{S}_{LT} = \hat{S}_L \odot \hat{S}_T = \begin{pmatrix} r_L & t_L \\ t_L^c & r_L^c \end{pmatrix} \odot \begin{pmatrix} r_T & t_T \\ t_T^c & r_T^c \end{pmatrix} = \frac{1}{1 - r_T r_L^c} \begin{pmatrix} \zeta_1 & t_L t_T \\ t_L^c t_T^c & \zeta_2 \end{pmatrix}, \tag{A23}$$

where $\zeta_1 = (r_T r_L^c - 1) r_L - r_T t_L t_L^c$, $\zeta_2 = (r_T r_L^c - 1) r_L^c - r_L^c t_T t_L^c$. The partial transmission $t_{L,T,R}$ and reflection $r_{L,T,R}$ coefficients of the fractional junctions are computed microscopically using solutions of the Bogolyubov equation [27,30]. Within the above assumptions and using the rule (A23), one obtains the net transmission coefficient t_{LR} through the whole $F_1I_2F_2I_3S_3$ multilayer as

$$t_{LR}(\varepsilon) = [\hat{S}_{LR}]_{12} = \frac{t_L t_T t_R}{Z_{LR}}, \tag{A24}$$

where

$$Z_{LR} = (1 - r_L r_T)(1 - r_R r_T) - r_L r_R t_T^2 \tag{A25}$$

and $r_{R(L)} = \sqrt{1 - t_{R(L)}^2}$. In practice, the partial transmission t_L, t_T, t_L, t_T and reflection r_L, r_T, r_R coefficients are not well known, therefore $\Upsilon_{\rm inj} = |t_{LR}(\varepsilon)|^2$ value is deduced directly from the injector's $I-V$ curve measured in the experiment. By setting

$$F_2^R(\varepsilon) = \frac{\Delta_2}{\sqrt{\varepsilon^2 - \Delta_2^2}} \tag{A26}$$

one obtains an equation determining the nonequilibrium gap Δ_2 in the form [13]

$$\ln\frac{T_c^0}{T} = \frac{7\zeta(3)}{8\pi^2}\frac{\Delta_2^2}{T^2} + 2\int_\Delta^{\hbar\omega_D} {\rm Re}\left\{\frac{1}{\sqrt{\varepsilon^2 - \Delta_2^2}}\right\}\delta f_\varepsilon d\varepsilon, \tag{A27}$$

where $\delta f_\varepsilon = f_\varepsilon - f_\varepsilon^F$ is the deviation of the electron distribution function f_ε from its equilibrium value f_ε^F. Equation (A27) is solved to obtain the dependence $\Delta_2(V_i)$ of the superconducting energy gap in the S_2 layer of the S_2F_1 sandwich situated in the middle of the multilayered structure versus the injector bias voltage V_i. The resulting dependence $\Delta_2(V_i)$ [see Fig. 2(a)] serves as an input in Eq. (23) when computing the critical current of the $S_1I_1S_2F_1$ acceptor junction versus the bias voltage V_i applied across the $S_2F_1I_2F_2S_3$ injector.

5. Solution of the Boltzmann equation

In this section we consider stationary (i.e., $\partial f_\varepsilon/\partial t = 0$) solutions of Eq. (A19) when the electron-phonon collision term $L_\varepsilon\{f\}$ has a more general form

$$L_\varepsilon\{f\} = L_\varepsilon^{(1)} + L_\varepsilon^{(2)} + L_\varepsilon^{(3)}, \tag{A28}$$

where

$$\begin{aligned}
L_\varepsilon^{(1)} &= \eta_{\rm EP}\int_\xi^{\omega_D+\xi}\frac{d\xi'}{\Delta^{k+2}}(\varepsilon'-\varepsilon)^{k+1}\left(1-\frac{\Delta^2}{\varepsilon\varepsilon'}\right)[(1-f)f'(1+N_{\varepsilon'-\varepsilon})-f(1-f')N_{\varepsilon'-\varepsilon}],\\
L_\varepsilon^{(2)} &= \eta_{\rm EP}\int_0^{\xi}\frac{d\xi'}{\Delta^{k+2}}(\varepsilon-\varepsilon')^{k+1}\left(1-\frac{\Delta^2}{\varepsilon\varepsilon'}\right)[f(1-f')(1+N_{\varepsilon-\varepsilon'})-(1-f)f'N_{\varepsilon-\varepsilon'}],\\
L_\varepsilon^{(3)} &= \eta_{\rm EP}\int_0^{\xi}\frac{d\xi'}{\Delta^{k+2}}(\varepsilon+\varepsilon')^{k+1}\left(1+\frac{\Delta^2}{\varepsilon\varepsilon'}\right)[ff'(1+N_{\varepsilon+\varepsilon'})-(1-f)(1-f')N_{\varepsilon-\varepsilon'}],
\end{aligned} \tag{A29}$$

where Δ is the energy gap of acceptor (we have omitted indices 1,2 for brevity) and $\eta_{\rm EP} = \pi|\lambda|/2$. The above integrals (A28), (A29) also are rewritten in a slightly different form

$$L_\varepsilon\{f\} = L_\varepsilon^{(1,0)} - L_\varepsilon^{(2,0)} - L_\varepsilon^{(3,0)} - f(L_\varepsilon^{(1,1)} - L_\varepsilon^{(2,1)} - L_\varepsilon^{(3,1)}), \tag{A30}$$

where

$$\begin{aligned}
L_\varepsilon^{(1,0)} &= \int_\xi^{\omega_D+\xi} d\xi' G_{-\varepsilon,\varepsilon'} f'(1+N_{\varepsilon'-\varepsilon}),\\
L_\varepsilon^{(1,1)} &= \int_\xi^{\omega_D+\xi} d\xi' G_{-\varepsilon,\varepsilon'} (f'+N_{\varepsilon'-\varepsilon}),\\
L_\varepsilon^{(2,0)} &= \int_0^{\xi} d\xi' G_{\varepsilon,-\varepsilon'} f' N_{\varepsilon-\varepsilon'},\\
L_\varepsilon^{(2,1)} &= \int_0^{\xi} d\xi' G_{\varepsilon,-\varepsilon'} (1-f'+N_{\varepsilon-\varepsilon'}),\\
L_\varepsilon^{(3,0)} &= \int_0^{\omega_D-\xi} d\xi' G_{\varepsilon,\varepsilon'} (1-f') N_{\varepsilon-\varepsilon'},\\
L_\varepsilon^{(3,1)} &= \int_0^{\omega_D-\xi} d\xi' G_{\varepsilon,\varepsilon'} [f'(1+N_{\varepsilon+\varepsilon'})+(1-f')N_{\varepsilon-\varepsilon'}];
\end{aligned} \tag{A31}$$

here, we have introduced the factor

$$G_{\varepsilon,\varepsilon'}^k = \frac{\pi|\lambda|}{2}\left(\frac{\varepsilon'+\varepsilon}{\omega_D}\right)^{k+1}\left(1+\frac{\Delta^2}{\varepsilon\varepsilon'}\right). \tag{A32}$$

The solution of the Boltzmann equation (A19) is obtained as follows. The zeroth-order iteration corresponds to the relaxation time approximation (RTA). The Boltzmann equation is rewritten as

$$I_0\tau_{\rm EP}\{[f^F_{\varepsilon_+}-f_\varepsilon]H_+ + [f^F_{\varepsilon_-}-f_\varepsilon]H_- + [1-f^F_{\tilde\varepsilon}-f_\varepsilon]\tilde H\} + f^F_\varepsilon - f_\varepsilon = 0 \tag{A33}$$

or

$$f^F_{\varepsilon_+}H_+I_0\tau_{\rm EP} + f^F_{\varepsilon_-}H_-I_0\tau_{\rm EP} + \tilde H I_0\tau_{\rm EP} - f^F_{\tilde\varepsilon}\tilde H I_0\tau_{\rm EP} + f^F_\varepsilon - f_\varepsilon - f_\varepsilon H_+ I_0\tau_{\rm EP} - f_\varepsilon H_- I_0\tau_{\rm EP} - f_\varepsilon\tilde H I_0\tau_{\rm EP} = 0. \tag{A34}$$

Solving Eq. (A36) with respect to f_ε we obtain

$$f_\varepsilon = \frac{f^F_\varepsilon + I_0\tau_{\rm EP}(\tilde H + f^F_{\varepsilon_+}H_+ + f^F_{\varepsilon_-}H_- - f^F_{\tilde\varepsilon}\tilde H)}{1 + I_0\tau_{\rm EP}(H_+ + H_- + \tilde H)}. \tag{A35}$$

The above solution (A35) serves as a zero-order input into the iterative scheme described below. More accurate solutions of the Boltzmann equation (A19) are obtained using iterations. There are two possible strategies for solving the Boltzmann equation more accurately. In either case, we consider Eq. (A35) as a zero-order approximation assuming $f_\varepsilon \to f_\varepsilon^{(0)}$. A technical complication arises due to presence of nonlinear terms in L_ε, originating from the products $\propto f_\varepsilon f_{\varepsilon'}$. The difficulty is fixed as follows. The electron-phonon collision integral L_ε is approximated by replacing the nonlinear terms containing products $\propto f_\varepsilon f_{\varepsilon'}$ with linear terms $f^a_\varepsilon f_{\varepsilon'}$ or $f_\varepsilon f^a_{\varepsilon'}$, where $f^a_{\varepsilon'}$ is an explicit approximate form of f_ε or $f_{\varepsilon'}$. A simple approach is to reduce the Boltzmann equation to an algebraic equation by replacing $f_\varepsilon f_{\varepsilon'} \to f_\varepsilon f^a_{\varepsilon'}$. As an initial guess (zero-order input) for $f^a_{\varepsilon'}$, we use the RTA function $f_\varepsilon \to f_\varepsilon^{(0)}$ defined by Eq. (A35). Then Eq. (A19) is easily solved analytically giving a better approximation $f_\varepsilon^{(1)}$ for f_ε. In the next step, we improve the approximation of L_ε by replacing

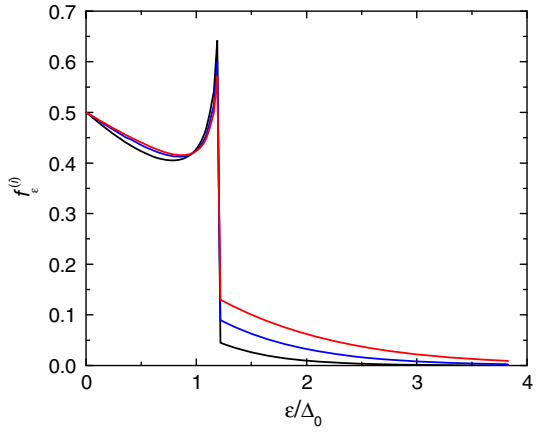

FIG. 7. The nonequilibrium electron distribution function $f_\varepsilon^{(i)}$ computed in successive iterations $i = 1, 2, 3$ (curves from bottom to top, respectively) by solving the Boltzmann equation for $eV_i = 2.2$, $T = 0.7$, $\Delta = 1$, as described in text.

$f_\varepsilon f_{\varepsilon'} \to f_\varepsilon f_{\varepsilon'}^{(1)}$ and solve the Boltzmann equation with the newly approximated L_ε, which gives another improvement in the precision of $f_\varepsilon^{(2)}$. The procedure is repeated several times, until the desired accuracy is accomplished.

Another path is to consider Eq. (A19) with the electron-phonon collision integral in explicit form, as the Fredholm integral equation of third or final kind using the following approximation to handle the products like $f_\varepsilon f_{\varepsilon'}$, entering the election-phonon integral. In the first iteration we use the RTA expression (A35) to replace the products $f_\varepsilon f_{\varepsilon'}|_{i=1} \to (f_\varepsilon^{(1)}) f_{\varepsilon'}$ entering the electron-phonon collision integral. Then the Boltzmann equation takes the form of the Fredholm integral equation of third or final kind, which is subject to iterative procedure. For the successive iterations $i > 1$, the products $f_\varepsilon f_{\varepsilon'}$ are replaced as $f_\varepsilon f_{\varepsilon'}|_i \to (f_\varepsilon^{(i-1)}) f_{\varepsilon'}$, where $f_\varepsilon^{(i-1)}$ represents the solution obtained in the previous iteration. If the iteration scheme converges, i.e., when at some i_0 we get $|f_\varepsilon^{i_0} - f_\varepsilon^{i_0-1}| \to 0$, we arrive at an accurate solution $f_\varepsilon = f_\varepsilon^{i_0}$ of the Boltzmann equation. In this work we use the methods described above. Although the second method based on solving the Fredholm integral equation is technically complicated, it gives a better convergence. The nonequilibrium electron distribution function obtained by solving the Boltzmann equation (A19) numerically is shown in Fig. 7 for the bias voltage $V_i = 2.2\Delta$ across the injector and for the successive iterations $i = 1, 2, 3$ (see curves from bottom to top, respectively).

6. The gap equation

The acceptor energy gap $\Delta_{1,2}$ dependence $\Delta_{1,2}(V_i)$ versus the injector bias voltage V_i is derived by solving the self-consistency equation

$$\frac{1}{\lambda} = \int_{\Delta_{1,2}}^{\omega_D} \mathrm{Re}\left\{\frac{1}{\sqrt{\varepsilon^2 - \Delta_{1,2}^2}}\right\}(1 - 2f_\varepsilon^{(1,2)})d\varepsilon. \quad \text{(A36)}$$

In a nonequilibrium superconductor we use the RTA expression (A35) serving as a zero-order input for the iterative schemes described above. Accurate solutions of the self-consistency equation (A36) describing the influence of the nonequilibrium effects on the energy gap $\Delta_{1,2}$ of the $S_{1,2}$ layers are obtained using the corresponding electron distribution function $f_\varepsilon^{(1,2)}$ that, in turn, is found by solving the Boltzmann equation (A19) numerically as described above. The threshold voltage V_{th} is defined as a value of V_i at which Δ_2 vanishes. The numeric solution of Eq. (A36) obtained allows one to deduce the threshold instability that occurs at certain values of V_i, corresponding to V_{th}. The magnitude of V_{th} depends on the resistance of the injector and the thicknesses of the $S_{1,2}$ layers, provided that all the other device parameters are fixed. The dependence of the threshold voltage $V_{\mathrm{th}}(R_{T(i)}/R_{T(a)})$ is shown in Fig. 3 in the main text.

[1] National Strategic Computing Initiative, White House executive order, http://www.hpcwire.com/off-the-wire/creating-a-national-strategic-computing-initiative/.

[2] D. S. Holmes, A. L. Ripple, and M. A. Manheimer, Energy-efficient superconducting computing—Power budgets and requirements, IEEE Trans. Appl. Supercond. **23**, 1701610 (2013).

[3] M. A. Manheimer, Cryogenic computing complexity program: Phase 1 Introduction, IEEE Trans. Appl. Supercond. **25**, 1301704 (2015).

[4] O. A. Mukhanov, Energy-efficient single flux quantum technology, IEEE Trans. Appl. Supercond. **21**, 760 (2011).

[5] Q. Herr, A. Herr, O. Oberg, and A. Ioannidis, Ultra-low-power superconductor logic, J. Appl. Phys. **109**, 103903 (2011).

[6] L. Ye, D. B. Gopman, L. Rehm, D. Backes, G. Wolf, T. Ohki, A. F. Kirichenko, I. V. Vernik, O. A. Mukhanov, and A. D. Kent, Spin-transfer switching of orthogonal spin-valve devices at cryogenic temperatures, J. Appl. Phys. **115**, 17C725 (2014).

[7] B. Niedzielski, S. Diesch, E Gingrich, Y. X. Wang, R. Loloee, W. P. Pratt, and N. O. Birge, Use of Pd-Fe and Ni-Fe-Nb as soft magnetic layers in ferromagnetic Josephson junctions for nonvolatile cryogenic memory, IEEE Trans. Appl. Supercond. **24**, 1800307 (2014).

[8] B. Baek, W. Rippard, S. Benz, S. E. Russek, and P. D. Dresselhaus, Hybrid superconducting-magnetic memory device using competing order parameters, Nat. Commun. **5**, 888 (2014).

[9] I. V. Vernik, V. Bol'ginov, S. Bakurskiy, A. A. Golubov, M. Y. Kupriyanov, V. V. Ryazanov, and O. A. Mukhanov, Magnetic Josephson junctions with superconducting interlayer for cryogenic memory, IEEE Trans. Appl. Supercond. **23**, 1701208 (2013).

[10] T. Golod, A. Iovan, and V. M. Krasnov, Single Abrikosov vortices as quantized information bits, Nat. Commun. **6**, 8628 (2015).
[11] M. G. Blamire and J. W. A. Robinson, The interface between superconductivity and magnetism: Understanding and device prospects, J. Phys. Condens. Matter **26**, 453201 (2014).
[12] M. Eschrig, Spin-polarized currents for spintronics: A review of current progress, Rep. Prog. Phys. **78**, 104501 (2015).
[13] V. F. Elesin and Yu. V. Kopaev, Superconductors with excess quasiparticles, Sov. Phys. Usp. **24**, 116 (1981).
[14] K. E. Gray, A superconducting transistor, Appl. Phys. Lett. **32**, 392 (1978).
[15] S. M. Faris, S. I. Raider, W. J. Gallagher, and R. E. Drake, Quiteron, IEEE Trans. Magn. **19**, 1293 (1983).
[16] B. D. Hunt, R. P. Robertazzi, and R. A. Buhrman, Gap suppression devices, IEEE Trans. Magn. **21**, 717 (1985).
[17] I. Iguchi and H. Kashimura, Nonequilibrium gap instability under tunnel injection of quasi-particles utilizing superconducting junctions with negative tunnel resistance, Solid State Commun. **58**, 499 (1986).
[18] I. Iguchi, Evaluation of the performance of superconducting nonequilibrium devices, J. Appl. Phys. **59**, 533 (1986).
[19] Y. Harada, N. Hirose, Y. Uzawa, S. Yoshimori, M. Sekine, and M. Kawamura, Analysis of quasi-particle injection 3-terminal device, Infrared Phys. **32**, 129 (1991).
[20] A. F. Morpurgo, T. M. Klapwijk, and B. J. van Wees, Hot electron tunable supercurrent, Appl. Phys. Lett. **72**, 966 (1998).
[21] N. Booth, P. Fisher, M. Nahum, and J. Ullom, A superconducting transistor based on quasiparticle trapping, Supercond. Sci. Technol. **12**, 538 (1999).
[22] G. P. Pepe, G. Ammendola, G. Peluso, A. Barone, L. Parlato, E. Esposito, R. Monaco, and N. E. Booth, Superconducting device with transistor-like properties including large current amplification, Appl. Phys. Lett. **77**, 447 (2000).
[23] F. Giazotto and J. P. Pekola, Josephson tunnel junction controlled by quasiparticle injection, J. Appl. Phys. **97**, 023908 (2005).
[24] I. P. Nevirkovets, A superconducting transistorlike device having good input-output isolation, Appl. Phys. Lett. **95**, 052505 (2009).
[25] I. P. Nevirkovets, O. Chernyashevskyy, G. V. Prokopenko, O. A. Mukhanov, and J. B. Ketterson, Superconducting-ferromagnetic transistor, IEEE Trans. Appl. Supercond. **24**, 1800506 (2014).
[26] I. P. Nevirkovets and M. A. Belogolovskii, Hybrid superconductor-ferromagnet transistor-like device, Supercond. Sci. Technol. **24**, 024009 (2011).
[27] A. I. Buzdin, Proximity effects in superconductor-ferromagnet heterostructures, Rev. Mod. Phys. **77**, 935 (2005).
[28] L. V. Keldysh, Diagram technique for nonequilibrium processes, Sov. Phys. JETP **20**, 1018 (1965).
[29] L. P. Gor'kov and G. M. Eliashberg, Superconducting alloys in a strong alternating field, Sov. Phys. JETP **29**, 698 (1969).
[30] N. B. Kopnin, *Theory of Nonequilibrium Superconductivity. International Series of Monographs on Physics* (Clarendon-Oxford University Press, 2001), p. 328.
[31] I. P. Nevirkovets, G. Prokopenko, O. A. Mukhanov, O. Chernyashevskyy, and J. B. Ketterson, *Investigation of Current Gain in Superconducting-Ferromagnetic Transistors, in 15th International Superconductive Electronics Conference, 2015* (ISEC, Nagoya, Japan, 2015).
[32] A. A. Golubov, M. Y. Kupriyanov, and V. F. Lukichev, Theory of Josephson effect in tunnel SNINS and SNIS structures, Fiz. Nizk. Temp. **10**, 799 (1984) [Low Temp. Sci., Ser. A **10**, 418 (1984)].
[33] M. Yu. Kupriyanov and V. F. Lukichev, The proximity effect in electrodes and the steady-state properties of Josephson SNS structures, Fiz. Nizk. Temp. **8**, 1045 (1982) [Low Temp. Sci., Ser. A **8**, 526 (1982)].
[34] S. E. Shafranjuk and J. B. Ketterson, Collective oscillations of the superconducting gap of multilayered Josephson junctions, Phys. Rev. B **72**, 212506 (2005).
[35] S. E. Shafranjuk and J. B. Ketterson, Resonant states of a double-barrier junction, Phys. Rev. B **72**, 024509 (2005).
[36] P. G. de Gennes, *Superconductivity of Metals and Alloys* (Benjamin, New York, 1966).
[37] S. Mayle, T. Gupta, S. Davis, V. Chandrasekhar, and S. E. Shafraniuk, Thermometry and thermal management of carbon nanotube circuits, J. Appl. Phys. **117**, 194305 (2015).
[38] S. Datta, *Electronic Transport in Mesoscopic Systems* (Cambridge University Press, Cambridge, UK, 1997).